CDF/PUB/ANAL/CDFR/8528
October 5, 2006

Measurement Of The Front Back Asymmetry In Top-Antitop Quark Pairs

Thomas A Schwarz[1]
University Of California-Davis
Dante Amidei[2]
University Of Michigan

Abstract

A method of reconstructing $t\bar{t}$ events in the lepton plus jets mode is applied to a measurement of the forward backward asymmetry in t-tbar pair production at CDF. The measurement is a test of discrete symmetries in t-tbar production and strong interactions at large Q^2, for which no other measurements exist. In the present data set it is potentially sensitive to the the presence of parity-violating production channels such as a massive Z′-like boson. Larger data sets will have sensitivity for an interesting charge asymmetry arising from pure QCD calculated at next-to-leading order. We measure the top quark forward-backward asymmetry for 695 pb^{-1} of CDF collision data, using 243 candidate $t\bar{t}$ lepton plus jets events in the high Pt lepton trigger streams. The kinematic fitter is used to reconstruct the production angle of the hadronic top quark in the p-pbar frame for each event, and the number of forward ($Cos(\Theta) > 0$) and backward ($Cos(\Theta) < 0$) events are counted. The top flavor is tagged by the lepton charge. The level of intrinsic front back asymmetry in the detector is estimated from large electroweak samples and found to be small. The predicted background contributions in the forward and backward hemispheres are subtracted. Bias and smearing from asymmetries in acceptance and reconstruction are corrected and the front-back asymmetry is calculated from the corrected front-back counts. The Standard Model predicts $A_{fb} = 0.038$ and we measure $A_{fb} = 0.20 \pm (0.11)^{stat} \pm (0.047)^{syst}$.

[1]schwarzt@fnal.gov
[2]amidei@umich.edu

Contents

1 Introduction

Symmetries play an important role in characterizing the behavior of elementary particles. In general, a symmetry implies a conservation law. For example, the invariance of the description of a physical system to linear translations of its spatial coordinates is associated with the conservation of linear momentum. Since the transformation can be over a continuous range of values, this is called a continuous symmetry.

A "discrete" symmetry involves a "swap" between fixed choices in certain variables. Three discrete symmetries of great importance in particle physics are:

- Charge Conjugation (C)
  - Transformation of particles to anti-particles.
  - Invariance implies conservation of charge.
- Parity (P)
  - Transformation of of coordinates to negative coordinates ($\vec{x} \rightarrow -\vec{x}$).
  - The physical system is invariant under mirror reflection.
- Time Reversal (T)
  - Transformation of time ($t \rightarrow -t$) in all expressions.
  - Invariance implies the physical process is reversible.

Although the weak interaction is a "symmetry violator", the strong interaction is currently believed to respect C,P, and T. However, there is very little test of this at high energies. Top quark physics at the Tevatron offers an interesting new forum for the study of discrete symmetries in the strong interaction. It is a strong process at very high energy. As will be shown in this note, we can completely reconstruct the $t\bar{t}$ kinematics, which enables the study of charge flow on a per event basis. With the charge in hand, we can define two asymmetries:

$$A_C = \frac{N_t(p) - N_{\bar{t}}(p)}{N_t(p) + N_{\bar{t}}(p)} \tag{1}$$

$$A_{fb} = \frac{N_t(p) - N_t(\bar{p})}{N_t(p) + N_t(\bar{p})} \tag{2}$$

where $N_i(j)$ = is the number of particle i traveling in the direction of particle j

- A_C is charge symmetry; a non-zero value for this implies a net top current flowing along the proton direction.

- The front-back asymmetry, A_{fb}, is the difference in the number of top quarks flowing forward and backward along the proton direction. This kind of asymmetry is typically associated with parity-violating weak production processes. This is not expected in strong interactions, though new production mechanisms that violate parity such as a Z' particle or Top Color could appear as a front back asymmetry in top production [9] [10]. If we assume that CP symmetry is conserved then $N_{\bar{t}}(p) = N_t(\bar{p})$ and the charge asymmetry is equal to the front back asymmetry.

Curiously, although the strong interaction conserves C, QCD predicts that strong interactions produce a net charge asymmetry in the pair production of top quarks at the Tevatron. Evaluated at leading order, heavy flavor pair production via $q\bar{q}$ or gg does not discriminate between quark and anti-quark. But at next-to-leading order, radiative corrections involving a virtual or real gluon in $q\bar{q} \rightarrow Q\bar{Q}$ lead to a difference in the production of Q and $\bar{Q}$, and consequently a charge asymmetry. The asymmetry originates from interference between initial and final state gluon brehmsstrahlung processes, shown in Figures 1a and 1b, which produce a negative asymmetry, and the "box diagram" with the Born processes shown in Figures 1c and 1d, which produce a positive asymmetry. The overall charge asymmetry is positive and predicted to be between $4-5\%$ by Kuhn and Rodrigo [33], and 3.8% by next-to-leading order Monte Carlo generator MC@NLO [21]. In this analysis we assume CP symmetry is conserved and therefore, the front-back asymmetry will be equal to the predicted charge asymmetry.

In this note, we present the measurement of A_{fb} in $t\bar{t}$ production, using 695 pb^{-1} of data. We first isolate a sample of top events and understand their backgrounds. We then develop a method to reconstruct the $t\bar{t}$ kinematics, and use it to measure the production angle of the top quark, the angle between the top quark and the proton beam. The top quark production angle is defined as:

$$\Theta = Tan^{-1}\left(\frac{P_t}{P_z}\right) \tag{3}$$

where P_z and P_t are the longitudinal and transverse momentum of the top quark in a coordinate system where the proton beam is the z-axis. The production angle distribution for the top quark, as predicted by the Monte Carlo simulation MC@NLO, is shown in Figure 2. The production angle is used to define and count the number of forward (in the proton direction) and backward (against the proton direction) events in the sample, and thus measure A_{fb}. The measured production angle is distorted from its true value by a number of experimental complications. Corrections for these effects are applied to the forward and backward counts to produce a measurement of A_{fb} which can be compared to the theoretical prediction. We now explain the experiment and method of measuring A_{fb} in detail.

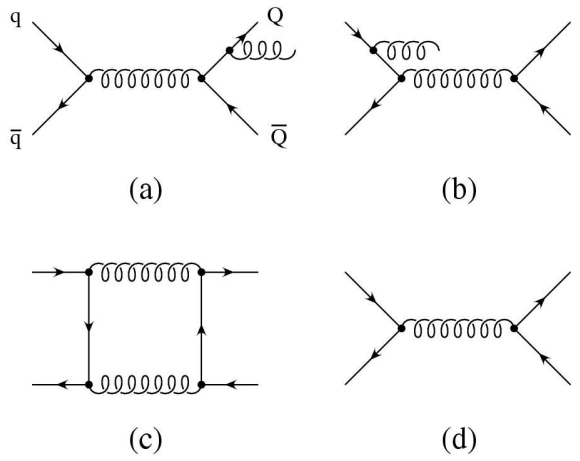

Figure 1: NLO Diagrams

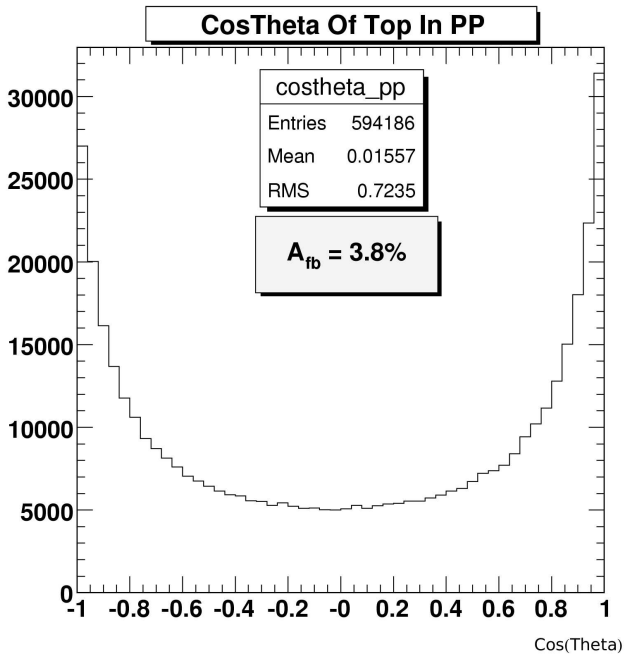

Figure 2: $Cos(\Theta)$ Distribution MC@NLO

2 Event Selection

This analysis is performed with $t\bar{t}$ events in the lepton plus jets channel as defined by the selection criteria in CDF Note 7372 [12]. A summary of the selection is shown below. This set of requirements produces roughly a 4 to 1 signal to background ratio.

- One tight high-P_t lepton
  First criteria for selection, which occurs at both trigger level and offline.
- Dilepton veto:
  Separates lepton plus jets from dilepton events.
- Z veto:
  Reduces the amount of background with Z-bosons.
- Primary vertex check:
  ensures the lepton and jets originate from the same process.
- $\not\!\!E_T \geq 20$ GeV:
  Selection based upon the presence of a neutrino in lepton plus jets events.
- ≥ 3 Tight and 1 Loose Jets:
  Reduces background by requiring the same number of jets as partons in a $t\bar{t}$ lepton plus jets event.
- ≥ 1 SecVtx "Tagged" jet:
  Rejects background processes without heavy flavor quarks present.

For 695 pb^{-1} of data collected at CDF the number of events that pass through event selection is 257. The breakdown of those events among the three high P_t lepton triggers is shown in Table 1.

Table 1: Events In Each Trigger For 695 pb^{-1}

	CEM	CMUP	CMX
N_{Events}	154	72	31
$\%OfTotal$	60.0%	28.0%	12%

Table 2: Signal And Background Estimates For 695 pb^{-1}

Jet Multiplicity	3.5 Jet	4 Jet	$\geq$5 Jets
EW	1.46±0.24	0.85±0.17	0.22±0.07
SingleTop	1.29±0.28	0.89±0.20	0.13±0.02
QCD	4.34±1.57	6.70±2.31	1.33±0.85
W+LF Mistags	9.38±1.85	4.95±0.98	0.48±0.11
Wc	2.47±0.76	1.11±0.50	0.04±0.04
W$c\bar{c}$	3.75±1.31	1.77±0.87	0.04±0.04
W$b\bar{b}$	8.40±2.66	3.71±1.72	0.26±0.26
Total Bkg	31.09±5.35	19.99±3.99	2.51±0.94
Data	91	128	38
$t\bar{t}$ Pred.	59.9	108.0	35.5

3 Backgrounds

Several kinds of processes without top quarks slip past our selection criteria. These events are backgrounds to the top quark signal and their presence biases and dilutes the measurement. Each background contribution for this analysis is estimated from the "Method 2" technique described CDF Note 7486 [17]. The predicted contribution for each background was calculated for an integrated luminosity of 319.5 pb^{-1}. The data sample for this analysis consists of 695 pb^{-1} of integrated luminosity. Since we believe the background fraction is independent of luminosity, the background content for this dataset is estimated by scaling the predicted amount from 319.5 pb^{-1} to 695 pb^{-1}. The number of events in data that pass our selection criteria and the background estimates are shown in Table 2. For this analysis, we assume the number of top events is equal to the difference between data and the background estimate.

4 Dataset Model

Models of the experimental dataset are used to simulate and understand our measurement. Generally, these models take the form of Monte Carlo simulations of the underlying physical process, called the "generator", and the response of the detector to that process, called the "CDF simulation". Information about both detector level objects, such as jets, and underlying physical objects, such as top quarks, is accessible in simulation. This allows comparisons between the elementary Standard Model objects and the objects actually observed at the detector level.

Each physical process predicted to be in our dataset is modeled by an appropriate simulation and normalized to the predicted number of events expected from "method II" [17]. The result is a complete model of the expected data collected at CDF and selected for this analysis. We discuss how the simulations are used and the tests we

perform to verify their accuracy.

4.1 Models For Each Process

The simulation used for each signal or background processes is described separately below. For a few of the background simulations the selection criteria is modified to improve statistics, but without changing predicted distributions. Table 3 is a summary of each dataset used in this analysis. Each model is a complete simulation of the initial collision in the event, the final state particles, and the response of the detector. Kinematics and angular distributions for all particles in the simulated events are entirely available and, thus the event selection, reconstruction, efficiencies, etc. can be completely simulated for every process.

Table 3: Datasets

Dataset	Type
bhel0d	CEM Triggered Data, Runs 138425-186598
bhmu0d	CMUP, CMX Triggered Data, Runs 138425-186598
bhel0h	CEM Triggered Data, Runs 190697-203799
bhmu0h	CMUP, CMX Triggered Data, Runs 190697-203799
ttopll	Herwig $t\bar{t}$, $M_t = 175.0 GeV$
ttopwl	Herwig $t\bar{t}$, $M_t = 175.0 GeV$
ttopkl	Pythia $t\bar{t}$, $M_t = 175.0 GeV$
ttophl	Herwig $t\bar{t}$, $M_t = 178.0 GeV$
ttopel	Pythia $t\bar{t}$, $M_t = 178.0 GeV$
ptop10	MC@NLO $t\bar{t}$, $M_t = 175.0 GeV$
atop7a, atopfb, ltop4n, ltop4m	Herwig+Alpgen W+4p
atoppb, atopjb, ltop2b, ltop5b	Herwig+Alpgen W$b\bar{b}$+2p
atoptb, atopmb, ltop2c, ltop5c	Herwig+Alpgen W$c\bar{c}$+2p
ltop3a, ltop7a	Herwig+Alpgen Wc+3p
mtopya	MadEvent+Pythia Single Top (S-Channel)
mytop(ta+ua)	MadEvent+Pythia Single Top (T-Channel)
wtop1w	Pythia WW
wtop1z	Pythia WZ
ztopcz	Pythia ZZ
atopxb	Herwig Z$\rightarrow \tau\tau$+2p

4.1.1 $t\bar{t}$ Signal

Two different generators are used to model $t\bar{t}$ signal events: Herwig and MC@NLO. Herwig generates events with a leading order matrix element calculation and uses a

parton shower program to simulate gluon radiation and the showering of jets [20]. MC@NLO generates events with a next-to-leading order matrix element calculation [21]. It is used in conjunction with Herwig which performs the parton shower simulation. In this analysis, we use MC@NLO to model kinematics and angular distributions for $t\bar{t}$ events. MC@NLO provides a better model of higher order QCD processes, including the NLO charge asymmetry. Herwig is used to generate a large number of events, 2 million, for simulating the effects that the detector, acceptance, and reconstruction have on the measurement. We expect these effects to be fairly independent of next-to-leading order effects, and by using Herwig for generation, the statistical error in the simulation of these effects is reduced by a factor of two.

4.1.2 Electroweak

Electroweak backgrounds are modeled by the Pythia Monte Carlo [19], which has a specialized treatment of final state hadronic interactions. Hard scattering processes are generated using Standard Model based calculations, and then a combination of analytical results and various QCD-string-based models simulate the multihadronic final states and parton evolution into jets.

4.1.3 Single Top

Single Top events are modeled at the generator level by MadEvent, for both s and t channels [22]. MadEvent is a multi-purpose, tree-level only event generator for a full range of collider processes including e^+e^-, ep, pp, $\gamma\gamma$, and $p\bar{p}$. It is a generator-only simulation and, therefore, is used in conjunction with Herwig to simulate parton showering into jets.

4.1.4 QCD

At this time, Monte Carlo simulations of QCD background events are not considered adequate models to predict the rare events that pass the $t\bar{t}$ selection. Instead, pretag data events with large $\not\!\!E_T$ and large lepton isolation are used as the model. Data events in this region are dominated by QCD and are assumed to be kinematically similar to background events in the signal region. Events in region C are required to have at least 3 tight jets and 1 loose jet and to boost statistics, instead of requiring a b-tagged jet, the jet with the highest positive mistag probability (as given by the mistag matrix [18]) is chosen as the b-tagged jet.

4.1.5 W + Heavy Flavor ($Wb\bar{b}$, $Wc\bar{c}$, and Wc)

W-boson plus heavy flavor events are modeled by Alpgen at the generator level and then passed to Herwig to simulate parton showering [23]. In W+jets events it is important to properly model the number of additional jets required by the selection criteria. Alpgen performs this accurately by including every diagram in a tree-level calculation. Herwig

is used to simulate parton showering, but all of the other final state radiation effects in Herwig are turned off, so that the final state jet multiplicity is completely determined by the ALPGEN calculation.

4.1.6 W + Light Flavor

W-boson plus light flavor events are modeled by Alpgen at the generator level, with Herwig used to simulate parton showering. As in case of the W + heavy Flavor background, we use Alpgen to accurately treat the multiparton processes that generate additional jets. The selection criteria is modified by treating the most "taggable" jet as a "tagged" jet and not requiring an actual tag in the event.

4.2 Study Of Simulation Performance

As will become clear in section 6, we rely on our simulations to understand the corrections necessary to relate A_{fb} as measured to the fundamental A_{fb} in $t\bar{t}$ production. We must therefore verify that the simulation correctly models any intrinsic differences in the forward and backward response of the detector.

4.2.1 Primary Vertex

The primary vertex is the collision point of the $p\bar{p}$ interaction as measured from the center of the detector. If the position of the primary vertex in Monte Carlo simulation is drastically different than data, our model for the geometric acceptance of jets and leptons will be skewed in η, and the production angle distribution of the top quark will not be simulated correctly.

In Figure 3, the primary vertex z-coordinate of simulated $t\bar{t}$ events are compared to primary vertex z-coordinate in the data used for this measurement. The background models are normalized to "method 2" values and the signal is normalized to the number of events found in the data minus the background prediction. The mean of the distribution for Monte Carlo and data are within statistical error, and the width differs by $< 4\%$. A slighly narrower distribution in the data is the result of a change in the beam profile since the production of the Monte Carlo. Although there is a slight shape difference, we believe that the overall agreement is good, and that the z vertex is adequately modeled for the analysis.

4.2.2 Front-Back Symmetry Of The Detector

The top event is composed of electrons, muons, and jets. Each of these is detected in a particular way, with particular apparatus. Therefore we can consider testing the simulation of electrons, muons, and jets separately to probe the modeling of the front-back acceptance of the detector. Fortunately, ideal samples are available in our high statistics inclusive high Pt lepton samples, which are dominated by leptonic vector boson decays. For example, $W \rightarrow e\nu$ events contain a high Pt electron and virtually nothing

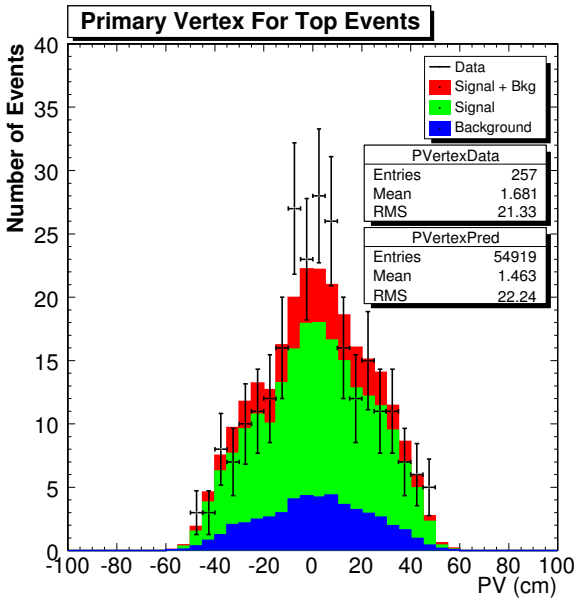

Figure 3: Primary Vertex z-coordinate for $t\bar{t}$ events

else. Comparing data and Monte Carlo for this process very selectively studies electron acceptance. With 70,000 identified $W \rightarrow e\nu$ decays, the η distribution of the electron can be compared to simulated $W \rightarrow e\nu$ decays with very good statistical precision over the entire detector, providing an accurate test of the simulation performance. We will examine the η distribution qualitatively, and also make a quantitative comparison. For our figure of merit, we will use A_{fb} where:

$$A_{fb} = \frac{N_{\eta>0} - N_{\eta<0}}{N_{\eta>0} - N_{\eta<0}} \tag{4}$$

and we will compare this A_{fb} between data and simulation. The samples of events for this test are selected from both Monte Carlo simulation and data with one isolated "tight" lepton, MET > 20 GeV, zero "tight" jets. It is assumed that there are very little or symmetric backgrounds to this selection criteria in collected data. The checks are performed with over 70,000 events for each check. For testing jets, the same method is applied, except a single tight jet is required in selection.

The results are shown in Table 4 and in Figures 4 to 9. The well known charge asymmetry from the vector boson production and decay is visible in the figures [24]. The asymmetry is opposite for positive and negative charged leptons, which demonstrates charge-parity is conserved in the detector. Comparing data and simulation bin-by-bin in η, we see that the simulation maps the detector in detail. The total A_{fb}'s are consistent to a few parts in 1000, and within the very small statistical error of the measurement. This is certainly adequate for our measurement in a top quark sample of approximately 300 events.

Table 4: A_{fb} Check On ±CEM Electrons, ±CMUP,CMX Muons and Jets

Check	A_{fb} Monte Carlo	A_{fb} Data	Difference
+CEM Electron	0.082±0.003	0.081±0.003	0.001±0.004
-CEM Electron	-0.086±0.003	-0.088±0.003	0.002±0.004
+CMUP Muon	0.051±0.004	0.047±0.004	0.004±0.006
-CMUP Muon	-0.044±0.004	-0.052±0.004	0.008±0.006
+CMX Muon	0.115±0.006	0.113±0.006	0.002±0.008
-CMX Muon	-0.111±0.006	-0.131±0.005	0.02±0.008
Lead Jet	0.006±0.006	0.003±0.007	0.002±0.009

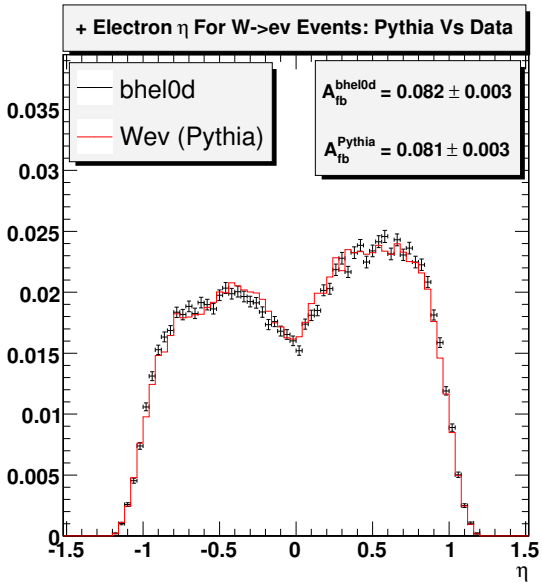

Figure 4: + Electron (CEM) η For W + 0 Jet Events

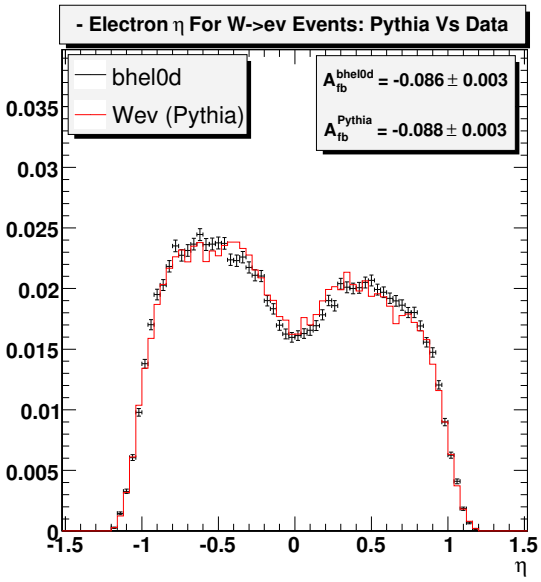

Figure 5: - Electron (CEM) η For W + 0 Jet Events

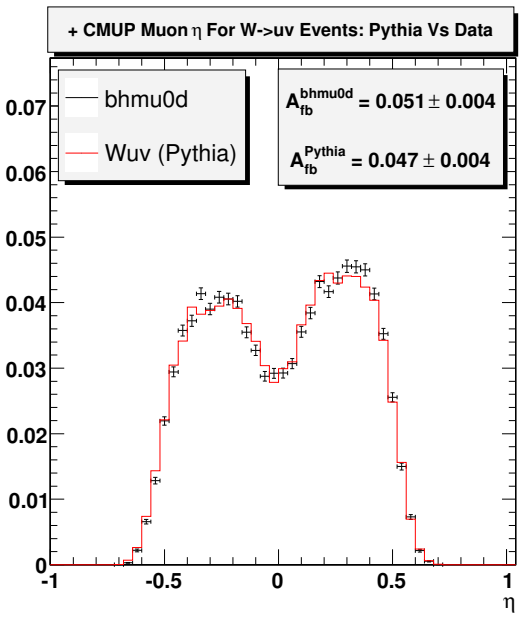

Figure 6: + Muon (CMUP) η For W + 0 Jet Events

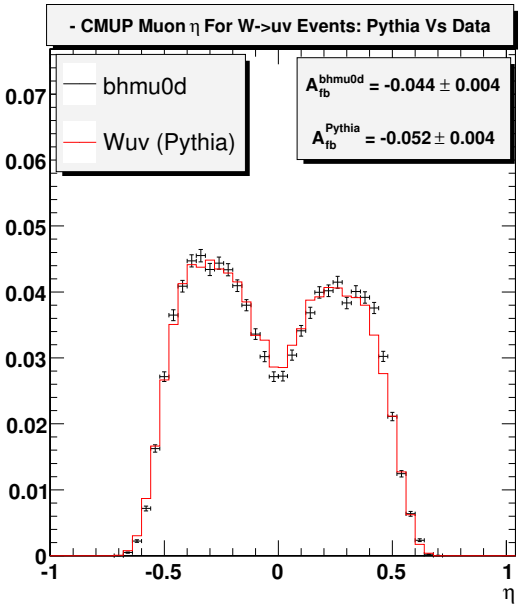

Figure 7: - Muon (CMUP) η For W + 0 Jet Events

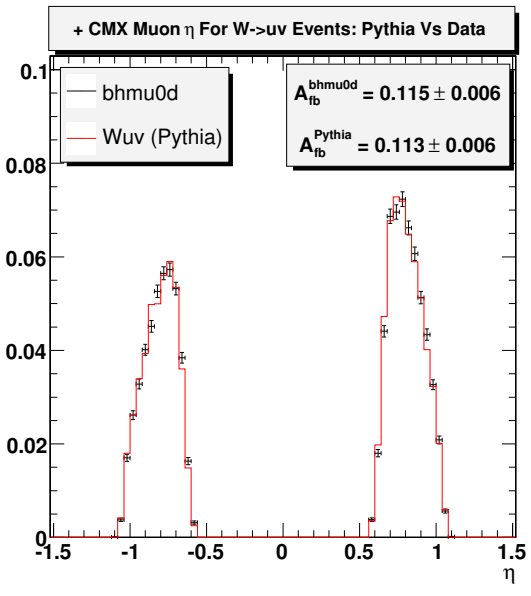

Figure 8: + Muon (CMX) η For W + 0 Jet Events

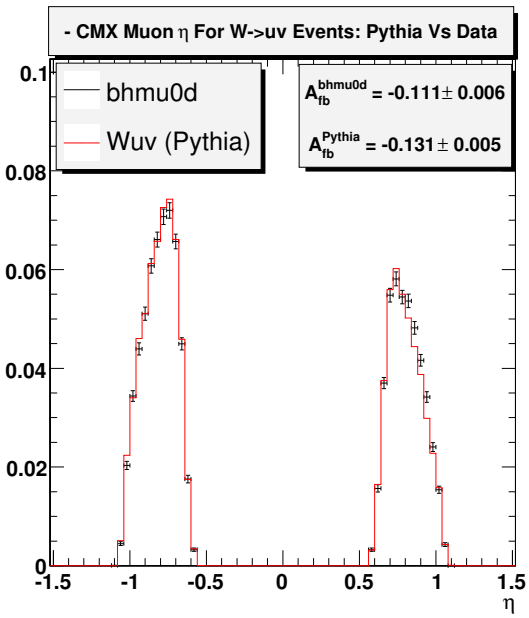

Figure 9: - Muon (CMX) η For W + 0 Jet Events

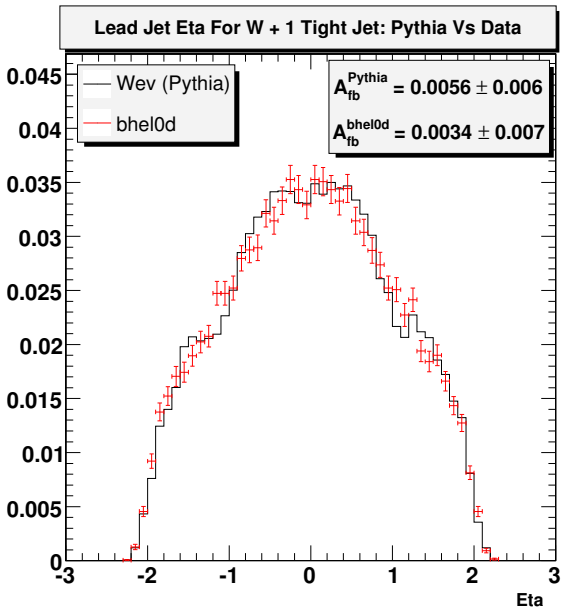

Figure 10: Leading Jet η For W + 1 Jet Events

5 Calculation Of The Front Back Asymmetry

5.1 $t\bar{t}$ Event Reconstruction

The measurement of A_{fb} will use the production angle of the top quark. The top quark is not directly observed in the detector, and therefore, we must reconstruct its momentum 4-vector from the final state particles: jets, charged leptons and neutrino. Unfortunately, we measure only the transverse component of the neutrino (in the $\not\!\!E_T$) and it is impossible to identify the parent quark of a jet based upon detector information. Because the type of parton cannot be identified by its jet, we cannot tell which jets came from which partons in a $t\bar{t}$ event. If we are to reconstruct the event we must find a method to choose the correct jet-parton assignments, as illustrated in Figures 11 and 12. We use an algorithm to match jets to the correct partons and reconstruct the full neutrino momentum by employing several constraints available in the "$t\bar{t}$ lepton plus jets hypothesis". This method allows us to reconstruct the complete kinematics of the $t\bar{t}$ final state.

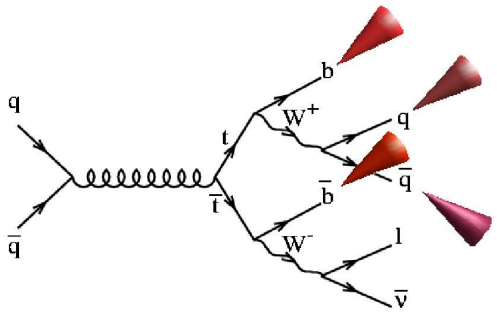

Figure 11: $t\bar{t}$ Lepton Plus Jets Event

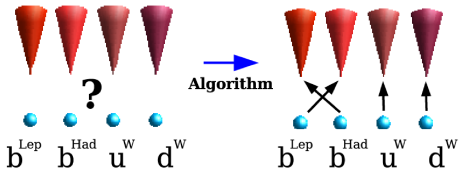

Figure 12: Matching Jets To Quarks

5.1.1 Matching Jets To Quarks And Reconstructing The Neutrino

The problem of reconstrucing the $t\bar{t}$ event is a combinatoric one: we must choose between a number of possible arrangements. The highest four energy jets in the event are assumed to come from the four quarks in the $t\bar{t}$ process. Matching four jets to four quarks leads to 24 possible combinations. This can be reduced by a factor of two since interchanging the two quarks from W-boson decay does not change the kinematics of the event.

Because we cannot measure the momentum of the event along the beam direction, we cannot infer the P_z of the neutrino from "missing E_z". However, we can calculate the neutrino P_z by requiring that the lepton and neutrino be consistent with the known mass of the W-boson. This calculation involves a quadratic equation and produces two solutions for the neutrino P_z. Both solutions are considered. Together with the jet assignments, the event has 24 possible combinations.

Our strategy is to test each combination for consistency with the "$t\bar{t}$ hypothesis". That hypothesis has four main components:

- The lepton and neutrino are decay products of a W-boson ($W \rightarrow l\nu$)
- Two jets are decay products of a W-boson ($W \rightarrow jj$)
- The lepton, neutrino, and a third jet are final states from a top quark decay ($t \rightarrow l\nu j$)
- The two jets from $W \rightarrow jj$ and a fourth jet are final states from the other top quark decay ($t \rightarrow jjj$)

The consistency of each combination with the $t\bar{t}$ hypothesis is assessed with a χ^2 test. The χ^2 equation is:

$$\chi^2 = \sum_{i=l,jets} \frac{(p_t^{i,meas} - p_t^{i,fit})^2}{\sigma_i^2} + \sum_{j=x,y} \frac{(p_j^{UE,meas} - p_j^{UE,fit})^2}{\sigma_j^2} + \frac{(M_{jj} - M_W)^2}{\Gamma_W^2} + \frac{(M_{lv} - M_W)^2}{\Gamma_W^2} + \frac{(M_{bjj} - M_{fit})^2}{\Gamma_t^2} + \frac{(M_{blv} - M_{fit})^2}{\Gamma_t^2} \quad (5)$$

While we are assessing the "goodness-of-fit" we can also take the opportunity to make modest corrections to the jet energies. The last four terms are the constraints. M_{jj} is the invariant mass of the two jets that must be consistent with the known W boson mass. M_{bjj} and M_{lvb} are the invariant masses of the hadronically decaying and leptonically decaying top quark side. These should be consistent with being equal, and their common value, M_{fit} is the best estimate of the top quark mass. M_{lv} is the mass of the lepton and the neutrino which must be consistent with the mass of a W boson. All four of the constraints are particle masses, and their weights are the theoretical decay width of the particle.

The first two terms are sums over lepton and jet transverse energies and "unclustered" energy, which is the energy in the event outside the $t\bar{t}$ interaction. These values are varied within their measured error. This improves resolution on jet energies, as well as the probability of finding the correct combination. The known top quark mass may also be used as a further constraint in the fit by setting $M_{fit} = M_{known}$.

The standard package MINUIT is used to vary the independent parameters and minimize the χ^2 for each possible combination of jet-parton assignments and neutrino solutions [25]. The combination with the lowest χ^2 is chosen as the best representative of the $t\bar{t}$ hypothesis for the event. Tests with Monte Carlo simulations show that the correct assignment is chosen 45% of the time, and this improves to 60 % in the constrained fit. In this analysis, any event with a $\chi^2 > 50$ is removed from the sample. This eliminates events that are badly measured as well as some fraction of background events.

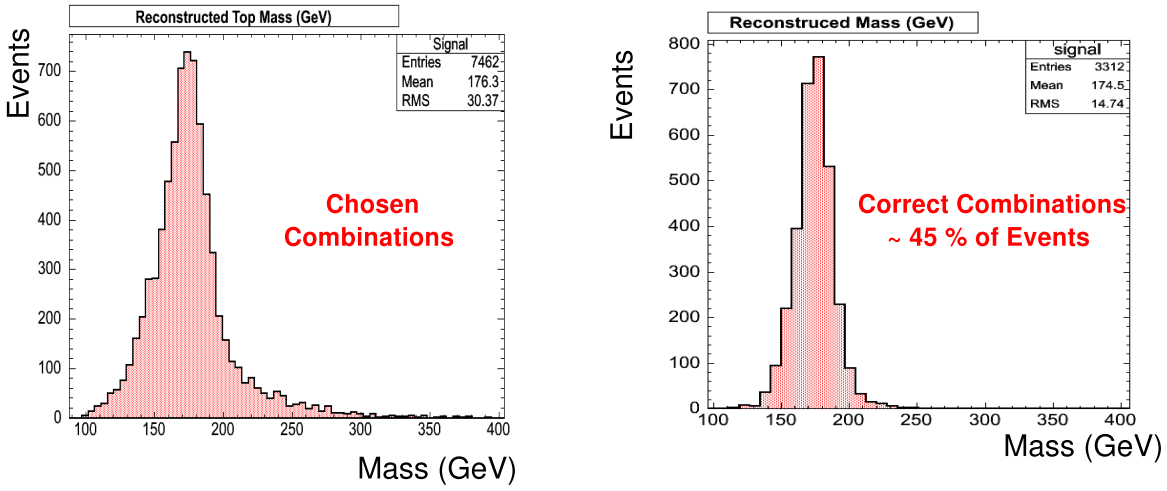

Figure 13: Reconstructed Mass For Chosen And Correct Combinations.

5.2 Reconstructed vs True Distributions

Figure 13 shows the reconstructed mass for the chosen and the correct jet-parton assignments in $t\bar{t}$ Monte Carlo with $M_t = 178$ GeV/c^2 and $\Gamma_t = 1.5$ GeV. Even for correct jet-parton assignments, the reconstructed distribution has a mean shifted from 178 GeV/c^2, and a smeared width much larger then 1.5 GeV. This is due to the measurement resolution of the energy of jets, leptons, and the missing energy. The chosen solution has events with both correct and incorrect jet-parton assignments. Incorrect jet-parton assignments further distort the mass distribution. These kinds of distortions will be an issue for any reconstructed distribution.

In order to draw conclusions about the "true" value of a quantity or measurement, the measured one will need to be corrected for these effects. The example shown here illustrates that the Monte Carlo simulation is a useful tool for this, as long as it is a faithful representation of reality. We discuss next how we use the Monte Carlo to assess the reconstruction and resolve some fundamental issues with our measurement.

5.3 Comparison Of Reconstructed Data To The Model

The algorithm has been applied to $t\bar{t}$ signal and background models as described in section 4, and 695 pb^{-1} of data collected at CDF. The signal and background models are normalized to the predicted values shown in Table 2 (53.6 background events and 203.4 signal events). We now compare a few example distributions in data and the model.

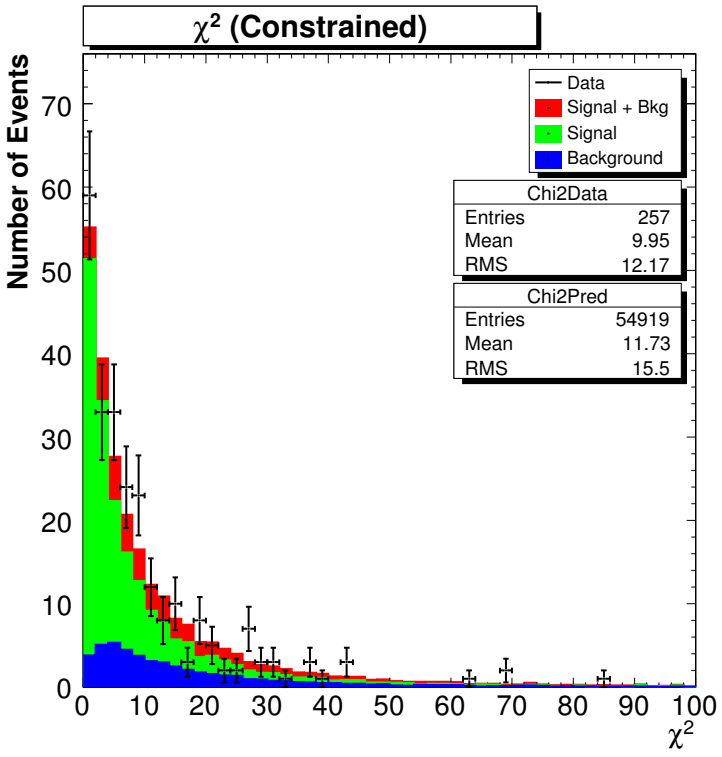

Figure 14: χ^2 Distribution

5.3.1 χ^2

The shape of the χ^2 distribution is a measure of the compatibility of events with the assumption that they originate from $t\bar{t}$ lepton plus jets processes. If the reconstruction of $t\bar{t}$ events is not well simulated by our model or normalization is incorrect, then the χ^2 distribution in data will diverge from predicted. The χ^2 distribution for data and our model is shown in Figure 14. The data and the model agree in shape and rate of decay far out into the tails. At the very outer edges of the tails ($\chi^2 > 50$) a few events in data appear. This is consistent with an integration of the number of events in the model predicted to have $\chi^2 > 50$. The good agreement between model and data is a high level check that event reconstruction of our model is an accurate simulation of event reconstruction in data.

5.3.2 Top Mass

The reconstruction algorithm is used by the CDF Top Mass Template Group to measure the top mass [26]. The distribution of the reconstructed mass should be another good quality control indicator for our analysis. The distribution of the reconstructed mass returned by the algorithm is shown in Figure 15 for our model and data. The shape of

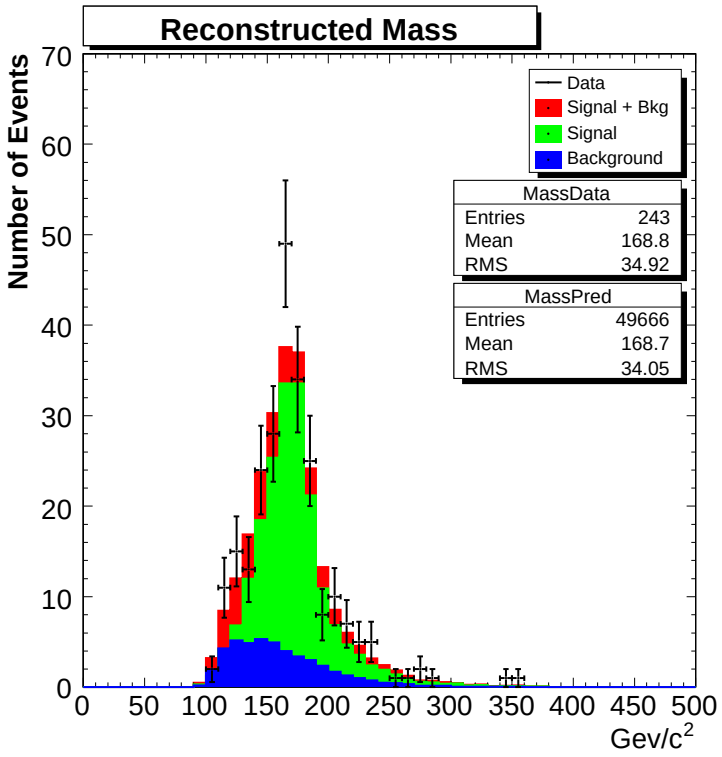

Figure 15: Reconstructed Top mass

the data at the low end of the spectrum follows the characteristic bump in the model which is due to backgrounds. At the peak of the distribution, which contains the bulk of events, the model and data follow the same sharp rise and decline. Even far out into the tails of the distribution, where little background exist, both model and data have similar shape. The good agreement between Monte Carlo and data, shown in 15, again suggest that our models are an accurate reflection of the data.

5.3.3 Top Quark Kinematics

To study quantities other than the mass, we can impose an additional constraint in the reconstruction that the top mass be consistent with our measured value. The default for our mass constrained reconstruction is $M_t = 175$ GeV/c^2, which is consistent with out measurement of $M_t = 173.4 \pm 2.8$ GeV/c^2 [26]. As discussed in section 5.1.1, this increases the number of correct jet-parton assignments by 15%. In all analysis following, this constraint is imposed.

The top quark transverse momentum is shown in Figure 16. The lack of events near $P_t = 0$ reflects the effect due to the kinematic cuts on jets, leptons, and missing energy in event selection: it is an acceptance effect. The data and our model are in good agreement over the entire spectrum.

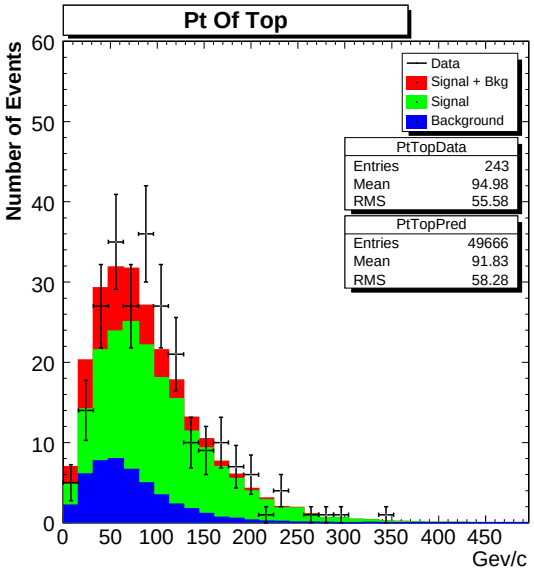

Figure 16: P_t Of Top

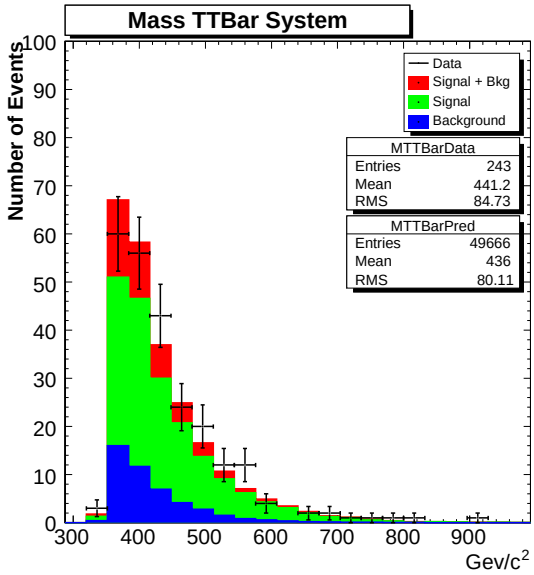

Figure 17: Invariant Mass $t\bar{t}$ System

The distribution of the invariant mass of the $t\bar{t}$ system is shown in Figure 17. No events are reconstructed with $M_{t\bar{t}} < 350$ due to the top mass constraint. The data and our model are consistent in the shape of the distribution from peak to tail: each show a slow exponential decline in number of events beginning at $M_{t\bar{t}} = 350$ with very few events with $M_{t\bar{t}} > 600$.

5.3.4 Top Production Angle

The top production angle Θ, is the angle between the outgoing top quark and the initial proton direction:

$$\Theta = tan^{-1}\left(\frac{P_t}{P_z}\right) \tag{6}$$

The use of a polar angle is somewhat unconventional in hadron collider physics. The usual choice is to transform to a closely related quantity called the rapidity:

$$y = \frac{1}{2} \cdot ln\left(\frac{E + P_z}{E - P_z}\right) \tag{7}$$

For a massless particle, y is approximately equal to the pseudo-rapidity. These variables are generally convenient because they are invariant against Lorentz transformations along the beamline. However, in our measurement we find that the polar angle is most convenient in studies of reconstruction, and we will develop our A_{fb} formalism around it.

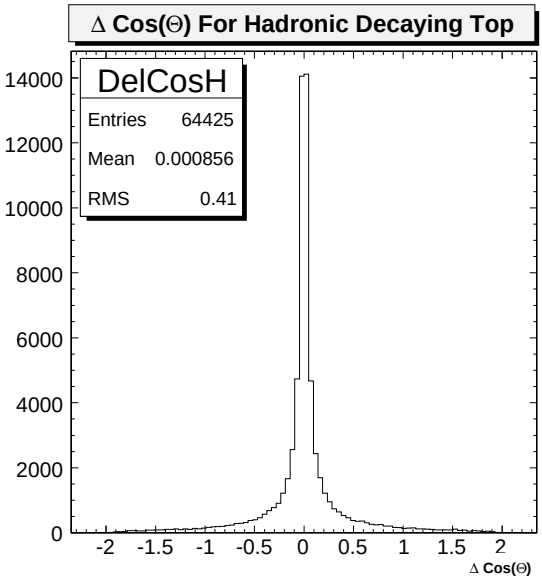

Figure 18: Resolution Of Cos(Θ), Hadronic Top Decay

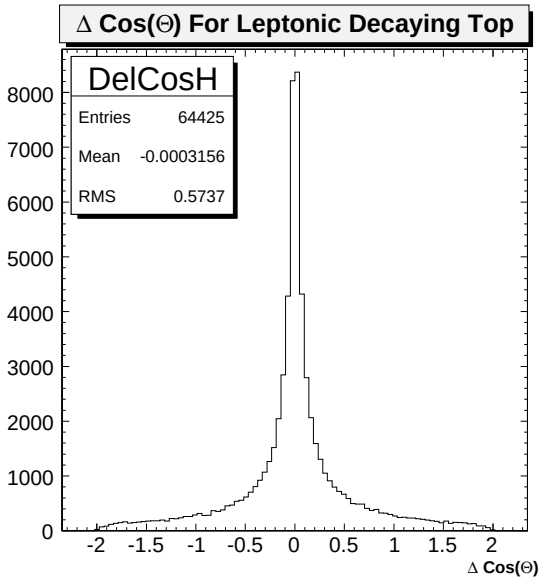

Figure 19: Resolution Of Cos(Θ), Leptonic Top Decay

5.3.5 Issues In The Production Angle Reconstruction

Because $Cos(\Theta)$ is central to our analysis, we study its reconstruction in further detail. To assess the accuracy of the reconstruction we compare the "true" value of the angle in top simulation to the reconstructed one. Our figure of merit is the difference:

$$\Delta Cos(\Theta) = Cos(\Theta)_{True} - Cos(\Theta)_{Recon} \tag{8}$$

The distribution of $\Delta Cos(\Theta)$ is shown in Figure 18 for the hadronically decaying top quarks in our model of $t\bar{t}$. This histogram shows that the majority of events are in a narrow peak with $|\Delta Cos(\Theta)| \leq 0.1$. The histogram illustrate that the algorithm effectively reconstructs the production angle of the top quark.

If charge conjugation symmetry is assumed in the production mechanism, then the production angle can be measured using either the hadronic or leptonic decaying top quark. $\Delta Cos(\Theta)$ for the leptonically decaying top quark is shown in Figure 19. The hadronically decaying top quark is more accurately reconstructed, with 1.4 times smaller RMS then leptonic decaying top quark. The reconstruction of the production angle of the leptonically decaying top quark is degraded by the lack of constraint in the longitudinal momentum. Because of this, we will use the hadronically decaying top quark to measure the production angle.

5.3.6 The Front-Back Asymmetry

Shown in Figure 20 is the production angle distribution for the hadronically decaying top quark, $(-Q_l) \cdot Cos(\Theta)$, where we have used the charge of the lepton, $-Q_l$, to infer

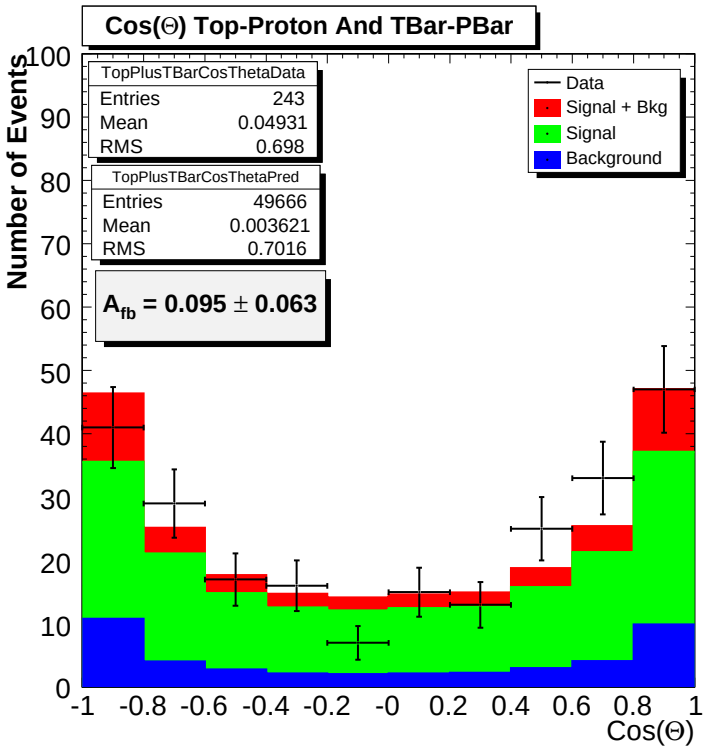

Figure 20: $(-Q_l) \cdot Cos(\Theta)$ Of Hadronic Decaying Top

the charge of the top quark. The forward backward asymmetry of this distribution is calculated by:

$$A_{fb} = \frac{N_{(-Q_l)\cdot Cos(\Theta)>0} - N_{(-Q_l)\cdot Cos(\Theta)<0}}{N_{(-Q_l)\cdot Cos(\Theta)>0} + N_{(-Q_l)\cdot Cos(\Theta)<0}} \tag{9}$$

The result in data and our model is:

$$A_{fb}^{data} = 0.095 \pm 0.063 \tag{10}$$

$$A_{fb}^{model} = 0.010 \pm 0.006 \tag{11}$$

The data shows a slight excess, which is nevertheless consistent with expectations within the large statistical error. In order to make a comparison to the theoretical prediction we must understand how to correct the reconstruction back to the "true" value. The corrections to the measurement are discussed in the next section.

6 Corrections To The Measured A_{fb}

In order to compare the measured front-back asymmetry to the theoretical prediction, we must account for any bias and smear of the $t\bar{t}$ asymmetry due to backgrounds, acceptance, and reconstruction. Our Monte Carlo model is expected to simulate these effects, and we use these simulations to understand and develop corrections.

Each correction is tailored to events in six different categories based upon the the high P_t lepton trigger and the lepton charge. These categories are $\pm CEM$, $\pm CMUP$, and $\pm CMX$. This is done to provide specific corrections to events which are detected with similar apparatus and selected with similar criteria.

Each individual effect and the corresponding corrections are described in the following sections.

6.1 Background Corrections

All non-signal processes dilute the measurement. In addition, several of backgrounds contain intrinsic asymmetries due to parity violating weak interactions, and these will bias the measurement.

Our remediation of this complication is a straight-forward subtraction. Each background model is run through reconstruction, giving an estimate of the ratio of forward to backward events. An absolute normalization is available from the background estimate described in section **??**. We then subtract the predicted number of forward and backward background events from the number measured in data.

The reconstructed production angle, $(-Q_l) \cdot Cos(\Theta)$, for the combined background model is shown in Figure 21. The contributions from the different background processes are stacked on one another. Compared to the $t\bar{t}$ signal model in Figure 20, the production angle in backgrounds is distributed much closer to the p and $\bar{p}$ direction ($Cos(\Theta) = \pm 1$). Therefore, the signal to background ratio will be larger then average at the outer edges of this distribution.

The predicted A_{fb} and normalization for each individual background is shown in Tables 5 through 10. The combined background asymmetry in all lepton categories for the reconstructed production angle distribution, $(-Q_l) \cdot Cos(\Theta)$, is:

$$A_{fb}^{Total\ Bkg} = -0.013 \pm 0.012$$

which is consistent with zero. Therefore, the largest effect the background has on the measurement is to dilute the $t\bar{t}$ signal.

The estimated number of forward and backward background events needs to be corrected separately for each kind of lepton. The number and uncertainty in each category is:

$$F_{bkg} = \frac{N_{bkg}}{2} \cdot (1 + A_{fb,\,bkg}) \tag{12}$$

$$\sigma^2_{F_{bkg}} = \sum_{i=bkg} \sigma^2_{A^i_{fb}} \cdot \frac{N^j_{bkg}}{2} \tag{13}$$

$$B_{bkg} = \frac{N_{bkg}}{2} \cdot (1 - A_{fb,\,bkg}) \tag{14}$$

$$\sigma^2_{B_{bkg}} = \sum_{i=bkg} \sigma^2_{A^i_{fb}} \cdot \frac{N^j_{bkg}}{2} \tag{15}$$

where,

N^i_{bkg} = # events in i^{th} background
N_{bkg} = Total # of events in lepton category
$A^i_{fb,\,bkg} = A_{fb}$ for i^{th} background
$A_{fb,\,bkg} = A_{fb}$ in lepton category

The error on background normalization will be considered as part of the systematic uncertainties in section 7. The measured number of forward and backward events is corrected for background contribution by subtracting the estimated contribution from the measurement.

$$F_{corr-bkg} = F_{meas} - F_{bkg} \tag{16}$$

$$\sigma^2_{F_{corr-bkg}} = \sigma^2_{F_{meas}} + \sigma^2_{F_{bkg}} \tag{17}$$

$$B_{corr-bkg} = B_{meas} - B_{bkg} \tag{18}$$

$$\sigma^2_{B_{corr-bkg}} = \sigma^2_{B_{meas}} + \sigma^2_{B_{bkg}} \tag{19}$$

where,

F, B_{meas} = Measured # F,B events in data
$\sigma_{F,B_{meas}}$ = Error on F, B_{meas} (Poisson)

The number of forward and backward events remaining after background subtraction is now treated as $t\bar{t}$ signal.

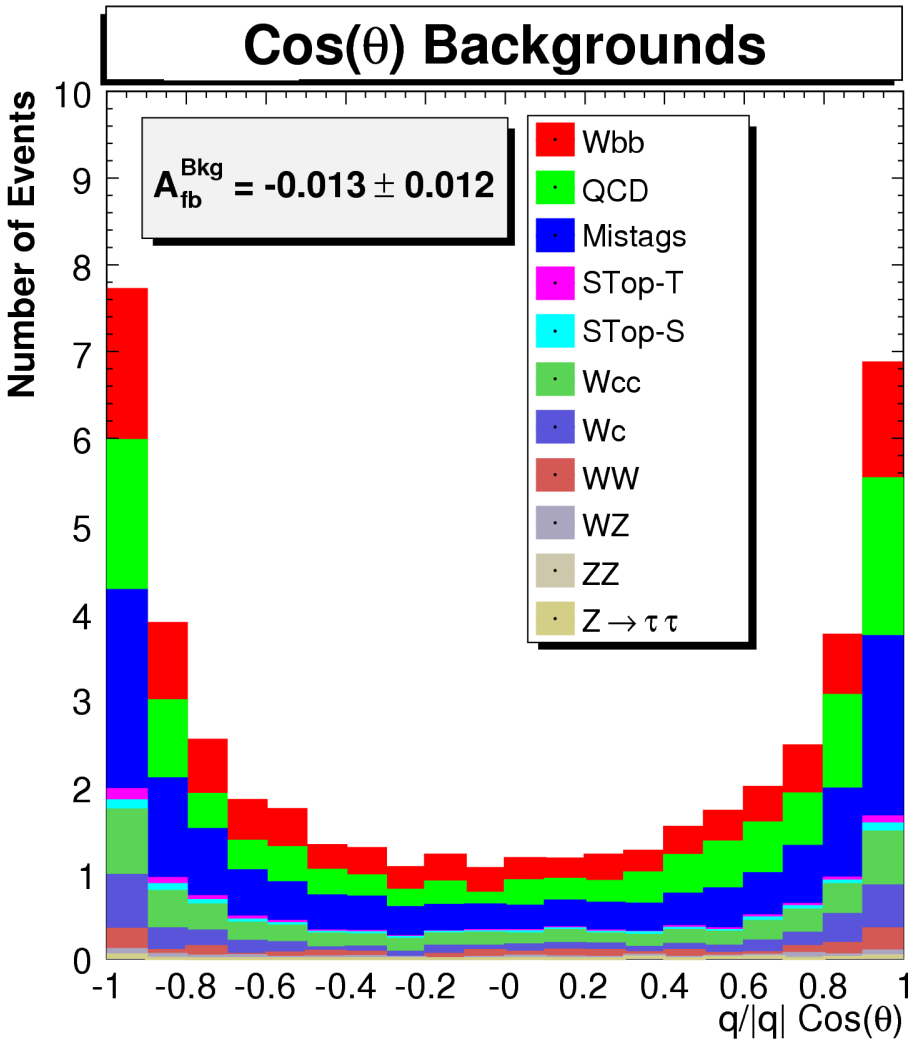

Figure 21: $-Q_l \cdot Cos(\Theta)$ For Backgrounds

Table 5: A_{fb}^{Bkg} +CEM Electron Events

Background	A_{fb}	N_{Events}^{Model}
QCD	-0.07±0.08	3.4
W+LF Mistags	0.028±0.016	3.5
W$b\bar{b}$	0.082±0.02	3.0
W$c\bar{c}$	0.07±0.04	1.3
Wc	-0.24±0.3	0.3
SingleTop-S	0.11±0.06	0.2
SingleTop-T	0.20±0.07	0.15
WW	-0.23±0.19	0.4
WZ	-0.10±0.18	0.1
ZZ	-0.20±0.44	0.01
Z$\rightarrow \tau\tau$	0.5±0.43	0.05
Combined	-0.01±0.02	12.3

Table 6: A_{fb}^{Bkg} -CEM Electron Events

Background	-CEM A_{fb}	N_{Events}^{Model}
QCD	0.10±0.08	3.5
W+LF Mistags	-0.082±0.016	3.5
W$b\bar{b}$	-0.11±0.02	3.0
W$c\bar{c}$	-0.07±0.04	1.2
Wc	-0.14±0.15	0.2
SingleTop-S	-0.06±0.06	0.2
SingleTop-T	-0.33±0.07	0.2
WW	0.07±0.19	0.4
WZ	0.15±0.13	0.2
ZZ	-0.23±0.27	0.02
Z$\rightarrow \tau\tau$	nil [a]	0.03
Combined	-0.04±0.02	12.3

[a] not enough events in MC

Table 7: A_{fb}^{Bkg} +CMUP Muon Events

Background	A_{fb}	N_{Events}^{Model}
QCD	-0.25±0.12	1.4
W+LF Mistags	0.018±0.022	2.1
W$b\bar{b}$	0.06±0.03	1.5
W$c\bar{c}$	0.02±0.06	0.8
Wc	0.05±0.07	1.1
SingleTop-S	-0.07±0.08	0.1
SingleTop-T	0.23±0.1	0.1
WW	0.11±0.23	0.3
WZ	0.0±0.27	0.07
ZZ	-0.67±0.3	0.01
Z$\rightarrow \tau\tau$	nil [a]	0.03
Combined	0.03±0.03	7.6

[a] not enough events in MC

Table 8: A_{fb}^{Bkg} -CMUP Muon Events

Background	A_{fb}	N_{Events}^{Model}
QCD	0.27±0.12	1.4
W+LF Mistags	-0.03±0.02	2.2
W$b\bar{b}$	-0.10±0.03	1.5
W$c\bar{c}$	-0.09±0.05	0.9
Wc	-0.04±0.08	0.7
SingleTop-S	-0.17±0.06	0.1
SingleTop-T	-0.06±0.07	0.1
WW	0.0±0.25	0.3
WZ	-0.29±0.26	0.07
ZZ	0.2±0.44	0.01
Z$\rightarrow \tau\tau$	nil [a]	0.01
Combined	0.01±0.03	7.3

[a] not enough events in MC

Table 9: A_{fb}^{Bkg} +CMX Muon Events

Background	A_{fb}	N_{Events}^{Model}
QCD	-0.07 ± 0.18	0.7
W+LF Mistags	0.09 ± 0.03	1.0
W$b\bar{b}$	0.12 ± 0.05	0.6
W$c\bar{c}$	0.04 ± 0.08	0.4
Wc	-0.05 ± 0.09	0.5
SingleTop-S	0.0 ± 0.14	0.04
SingleTop-T	0.12 ± 0.14	0.05
WW	-0.27 ± 0.29	0.2
WZ	0.43 ± 0.34	0.03
ZZ	nil [a]	0.0
Z→ $\tau\tau$	nil [b]	0.0
Combined	-0.03±0.05	3.5

[a]not enough events in MC
[b]not enough events in MC

Table 10: A_{fb}^{Bkg} -CMX Muon Events

Background	A_{fb}	N_{Events}^{Model}
QCD	-0.29 ± 0.16	0.7
W+LF Mistags	-0.05 ± 0.03	1.0
W$b\bar{b}$	-0.03 ± 0.05	0.6
W$c\bar{c}$	-0.12 ± 0.08	0.4
Wc	-0.07 ± 0.12	0.5
SingleTop-S	0.0 ± 0.14	0.04
SingleTop-T	-0.18 ± 0.17	0.05
WW	0.33 ± 0.54	0.2
WZ	-0.14 ± 0.37	0.03
ZZ	0.0 ± 0.71	0.0
Z→ $\tau\tau$	nil [a]	0.0
Combined	-0.1±0.05	3.3

[a]not enough events in MC

6.2 Acceptance Corrections

The reconstruction of the top quark production angle requires almost every component of the detector: hadronic and electromagnetic calorimeters, muon chambers, tracking chambers, and silicon tracking. Front-back asymmetries in detection efficiencies or acceptance will translate into an apparent asymmetry in measurement, which we will need to correct.

We use $t\bar{t}$ model to study how selection and the detector effect the measured number of forward and backward events. We define the selection efficiencies as follows:

$$\epsilon_F = \frac{F_{sel}}{F_{gen}} \tag{20}$$

$$\epsilon_B = \frac{B_{sel}}{B_{gen}} \tag{21}$$

where,

F, B_{sel} = # F,B events selected in MC
F, B_{gen} = # F,B events generated from MC

Using these efficiencies, the number of forward and backward events selected for analysis can be related to those generated by the matrix multiplication:

$$\begin{bmatrix} F_{sel} \\ B_{sel} \end{bmatrix} = M_A \cdot \begin{bmatrix} F_{gen} \\ B_{gen} \end{bmatrix} \tag{22}$$

where,

$$M_A = \begin{bmatrix} \epsilon_f & 0 \\ 0 & \epsilon_b \end{bmatrix}$$

Since different lepton types are detected in separate apparatus with different geometries we study ϵ_f and ϵ_b in each case. Using 2 million $t\bar{t}$ simulated events, six matrices are formed for each of the six lepton categories; ±CEM electron, ±CMUP Muon, and ±CMX Muon. The elements of M_A for each lepton category are shown in Table 11.

Defined in this way, these efficiencies are actually very close to the overall acceptance efficiency of the lepton plus jets selection. The efficiencies are low magnitude because most of the generated Monte Carlo events are $t\bar{t}$ dilepton and all-hadronic events, which our selection criteria removes. Dilepton and all-hadronic events that do pass selection are considered part of our sample. All categories show a small differences between the forward and backward efficiencies except events with a +CMUP muon.

Table 11: Elements Of M_A

Event Type	ϵ_f	ϵ_b
+CEM	0.0116±0.0001	0.0114±0.0001
-CEM	0.0113±0.0001	0.0120±0.0001
+CMUP	0.0100±0.0001	0.0100±0.0001
-CMUP	0.0090±0.0001	0.0100±0.0001
+CMX	0.0116±0.0001	0.0114±0.0001
-CMX	0.0113±0.0001	0.0120±0.0001

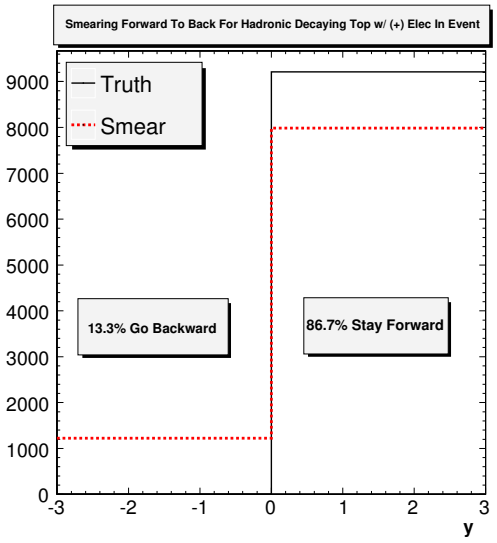

Figure 22: Demonstration Of Forward To Backward Smearing For +CEM Electron.

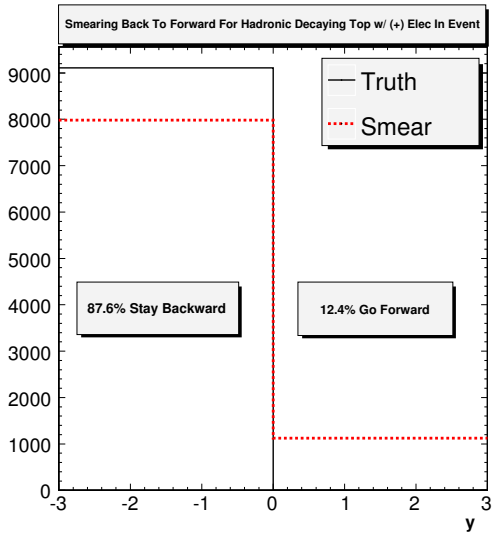

Figure 23: Demonstration Of Backward To Forward Smearing For +CEM Electron.

6.3 Reconstruction Corrections

Mismeasured jet energies, incorrect jet-quark assignments, and charge misidentification contribute to a smearing effect in the reconstructed production angle, which can translate into a change in the populations of events measured forward and backward. This is demonstrated in Figures 22 and 23 for Monte Carlo Top events with a +CEM electron. We see that the effect of reconstructing into the wrong hemisphere occurs for 12 to 13% of top quarks.

With this Monte Carlo based determination of smearing, we can correct out measurement using a further elaboration of our matrix formalism. We define a smearing matrix as follows. Let

$$\begin{bmatrix} F_{meas} \\ B_{meas} \end{bmatrix} = M_R \cdot \begin{bmatrix} F_{sel} \\ B_{sel} \end{bmatrix} \tag{23}$$

where,

$$M_R = \begin{bmatrix} \lambda_{ff} & \lambda_{bf} \\ \lambda_{fb} & \lambda_{bb} \end{bmatrix}$$

The elements of M_R are defined as follows:

$$\begin{aligned} \lambda_{ff} &= \frac{F_{sel}(F)}{F_{sel}} & \lambda_{bf} &= \frac{F_{sel}(B)}{B_{sel}} \\ \lambda_{fb} &= \frac{B_{sel}(F)}{F_{sel}} & \lambda_{bb} &= \frac{B_{sel}(B)}{B_{sel}} \end{aligned} \tag{24}$$

where,

$$\begin{aligned} F_{sel} &= \#\text{ Forward events selected (as in eqn 20)} \\ B_{sel} &= \#\text{ Backward events selected (as in eqn 20)} \\ F_{sel}(F) &= \#\text{ Selected forward events reconstructed forward} \\ F_{sel}(B) &= \#\text{ Selected forward events reconstructed backward} \\ F_{sel}(F) &= \#\text{ Selected backward events reconstructed forward} \\ F_{sel}(F) &= \#\text{ Selected backward events reconstructed backward} \end{aligned}$$

Using our Monte Carlo model we can estimate the elements of M_R for each category of lepton. The errors are binomial because each event is reconstructed either forward or backward:

$$\sigma_{M_R} = N_{events} \cdot p \cdot (1 - p) \tag{25}$$

where p is λ_{ij}.

The off-diagonal element of Table 12 reproduce the conclusion from Figures 22 and 23.: between 13 and 15% of events are reconstructed in the wrong direction. The matrices also show a slight difference in the off-diagonal elements. This is because the reconstructed distribution in our Monte Carlo model is dependent on event selection. As seen in Table Table 11, event selection is slightly asymmetric. This skews the production angle distribution in the $t\bar{t}$ model, which propagates into the reconstructed distribution.

Table 12: Elements Of M_R

Event Type	λ_{ff}	λ_{bf}	λ_{fb}	λ_{bb}
+CEM	0.852±0.009	0.147±0.009	0.136±0.009	0.876±0.009
-CEM	0.867±0.009	0.134±0.009	0.144±0.009	0.856±0.009
+CMUP	0.848±0.010	0.152±0.010	0.143±0.010	0.857±0.010
-CMUP	0.869±0.010	0.131±0.010	0.147±0.010	0.852±0.010
+CMX	0.848±0.010	0.152±0.010	0.143±0.010	0.857±0.010
-CMX	0.869±0.010	0.131±0.010	0.147±0.010	0.852±0.010

6.4 Total Correction To The Measured A_{fb}

With the understanding of acceptance and reconstruction bias in hand, we can develop an overall formalism for correcting the measured A_{fb} back to the true A_{fb} of $t\bar{t}$ production. Matrices M_A and M_R are multiplied together to create a relationship between the background corrected number of forward and backward events and the true number of forward and backward events generated in Monte Carlo. We will call the corrected values that are comparable to the number of events generated: F_{corr} and B_{corr}.

$$\begin{bmatrix} F_{corr-bkg} \\ B_{corr-bkg} \end{bmatrix} = M_R \cdot M_A \cdot \begin{bmatrix} F_{corr} \\ B_{corr} \end{bmatrix} \tag{26}$$

The combined matrix formed by multiplication of M_A and M_R is then inverted so that we can solve for the corrected values.

$$\begin{bmatrix} F_{corr} \\ B_{corr} \end{bmatrix} = [M_R \cdot M_A]^{-1} \cdot \begin{bmatrix} F_{corr-bkg} \\ B_{corr-bkg} \end{bmatrix} \tag{27}$$

We define the correction matrix M_C, where:

$$M_C = [M_R \cdot M_A]^{-1} = \begin{bmatrix} M_0 & M_1 \\ M_2 & M_3 \end{bmatrix} \tag{28}$$

Using the values from Tables 11 and 13, the elements of the correction matrix are calculated, shown in Table 13.

We apply our correction matrices to the background corrected values from equations 18 and 16 . The corrected number of forward and backward events and their uncertainty is:

$$F_{corr} = F_{corr-bkg} \cdot M_0 + B_{corr-bkg} \cdot M_1 \tag{29}$$

$$\sigma^2_{F_{corr}} = \sigma^2_{F_{corr-bkg}} \cdot M_0^2 + \sigma^2_{B_{corr-bkg}} \cdot M_1^2 \tag{30}$$

Table 13: Elements Of M_C

Event Type	M_0	M_1	M_2	M_3
+CEM	110.1	-18.0	-16.5	110.4
-CEM	111.9	-15.8	-17.6	106.3
+CMUP	171	-29.6	-27.4	173.2
-CMUP	177.4	-25.9	-29.4	170.8
+CMX	496.9	-99.9	-84.5	528.4
-CMX	513.1	-71.5	-82.6	500.9

$$B_{corr} = F_{corr-bkg} \cdot M_2 + B_{corr-bkg} \cdot M_3 \tag{31}$$
$$\sigma^2_{B_{corr}} = \sigma^2_{F_{corr-bkg}} \cdot M_2^2 + \sigma^2_{B_{corr-bkg}} \cdot M_3^2 \tag{32}$$

These values are used to calculate the final corrected asymmetry that may be compared to theoretical prediction.

$$A_{fb}^{corr} = \frac{F_{corr} - B_{corr}}{F_{corr} + B_{corr}} \tag{33}$$

$$\begin{aligned} \sigma^2_{A_{fb}^{corr}} = \; & \sigma^2_{F_{corr}} \cdot \left(\tfrac{2B_{corr}}{F_{corr}+B_{corr}}\right)^2 + \sigma^2_{B_{corr}} \cdot \left(\tfrac{2F_{corr}}{F_{corr}+B_{corr}}\right)^2 \\ & + \; 8 \cdot |F_{corr} \cdot B_{corr}| \cdot |M_0 \cdot M_2| \cdot \sigma^2_{F_{corr-bkg}} \\ & + \; \tfrac{|M_1 \cdot M_3|}{F_{corr}+B_{corr}} \cdot \sigma^2_{B_{corr-bkg}} \end{aligned} \tag{34}$$

6.4.1 Validation Of The Correction Procedure

Does this procedure really correct a measured asymmetry back to the true value? We will verify this by constructing Monte Carlo simulated samples with known asymmetries, applying our procedure, and comparing the results with the inputs.

Simulated A_{fb}
Our MC@NLO simulation has a real asymmetry which is probably too small to measure with our current dataset. To test realistic values, we need the statistics and flexibility of our Herwig model. It has no intrinsic asymmetry, but samples with asymmetry can be created by reweighting the production angle distribution of the top quark at the parton level.

The $Cos(\Theta)$ distribution from generic Herwig is shown in Figure 24. Let x represent the production angle, $f(x)$ is a 9th order polynomial fit to the distribution in Figure 24, and $a(x)$ is the asymmetric function we wish to add to $f(x)$ to produce our simulated asymmetric distribution. To produce the "new" distribution, $f(x) + a(x)$,

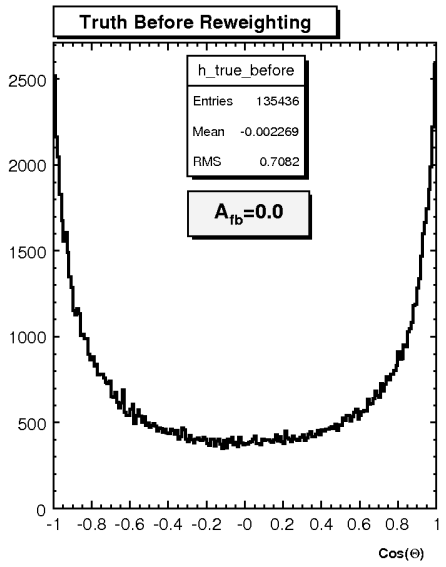

Figure 24: True $Cos(\Theta)$ Before Reweighting To 10%

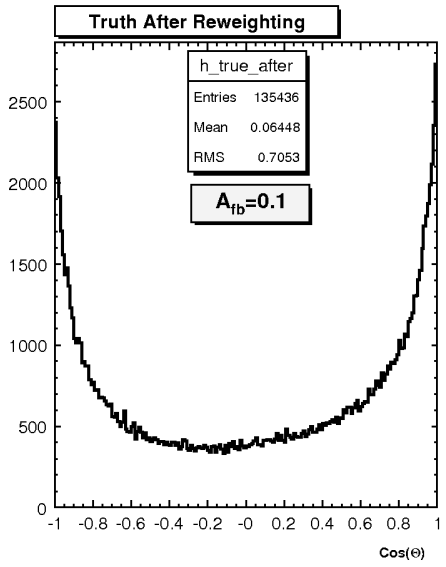

Figure 25: True $Cos(\Theta)$ After Reweighting To 10%

we can reweight each event in the generic Herwig distribution by the value calculated in equation 35.

$$\text{New Weight is: } \frac{\text{f(x)} + \text{a(x)}}{\text{f(x)}} \tag{35}$$

$$\begin{aligned} x &= Cos(\Theta) \\ f(x) &= \textstyle\sum_{i=0}^{9} \alpha_i \cdot x^i \text{ (Polynomial fit to original symmetric distribution)} \\ a(x) &= A_{fb} \cdot x \end{aligned}$$

This produces a $t\bar{t}$ production angle distribution which adds an asymmetry of magnitude A_{fb} to the symmetric form of the original.

As an example, the production angle distribution for events with a +CEM electron are reweighted to produce a 10% asymmetry. These events are then passed through event selection and reconstruction. The true and reconstructed distribution, before reweighting, are shown in Figures 24 and 26, and the reweighted distributions are shown in Figures 25 and 27. The reweighted true distribution has a linear increase from $Cos(\Theta) = -1$ to $Cos(\Theta) = 1$ and a 10% asymmetry. Both original and reweighted reconstructed distributions show the effects of smearing. The high peaks at the edges of both distributions, near $Cos(\Theta) = \pm 1$, are eroded into the center, and the reweighted distribution has a diluted asymmetry of 7.6%. The matrix M_R will be used to correct for these effects.

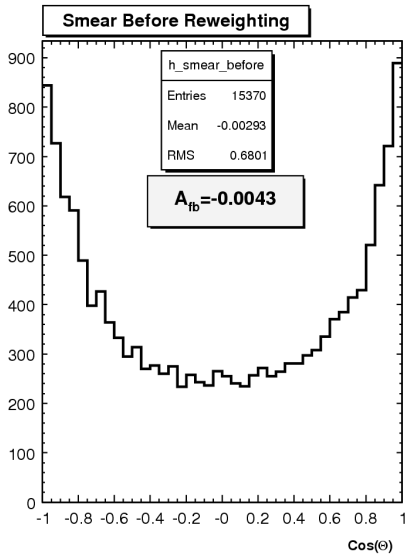

Figure 26: Reconstructed $Cos(\Theta)$ Before Reweighting To 10%

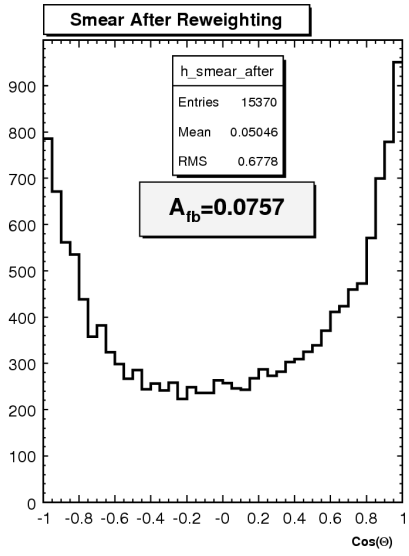

Figure 27: Reconstructed $Cos(\Theta)$ After Reweighting To 10%

Correcting Simulated A_{fb}

This technique is applied to produce a range of asymmetries between ± 0.40. The A_{fb} is measured in each sample and then corrected using the matrices derived in section 6.4.

The results of our test are shown in Tables 15, 16, and 17 for ±CEM,±CMUP,and ±CMX categories. The combined result is shown in Table 14. The errors in the tables are entirely statistical. We conclude that, to first order, our correction procedure takes the measured A_{fb} back to the "true" values. A small over correction which increases with the size of A_{fb} may be evident but, the effect is small and will be treated as a systematic error for our measurement.

Table 14: Combined Bias Check

Input A_{fb}	Combined Measured A_{fb}
-0.4	-0.428±0.006
-0.2	-0.212±0.006
-0.1	-0.104±0.006
-0.05	-0.051±0.006
0.0	0.003±0.006
0.05	0.057±0.006
0.1	0.11±0.006
0.2	0.221±0.006
0.4	0.436±0.006

Table 15: Bias Check For CEM Case

Input A_{fb}	A_{fb}^{meas} +CEM	A_{fb}^{meas} -CEM
-0.4	-0.431±0.011	-0.414±0.012
-0.2	-0.215±0.012	-0.199±0.012
-0.1	-0.106±0.012	-0.094±0.012
-0.05	-0.053±0.012	-0.041±0.012
0.0	0.002±0.012	0.012±0.012
0.05	0.057±0.012	0.065± 0.012
0.1	0.109±0.012	0.118 ± 0.012
0.2	0.217±0.012	0.228±0.011
0.4	0.431±0.011	0.439±0.011

Table 16: Bias Check For CMUP Case

Input A_{fb}	A_{fb}^{meas} +CMUP	A_{fb}^{meas} -CMUP
-0.4	-0.431±0.015	-0.40±0.015
-0.2	-0.21±0.015	-0.19±0.015
-0.1	-0.102±0.015	-0.090±0.015
-0.05	-0.047±0.015	-0.037±0.015
0.0	0.007±0.015	0.015±0.015
0.05	0.062±0.015	0.067±0.015
0.1	0.117±0.015	0.12±0.015
0.2	0.230±0.015	0.231±0.015
0.4	0.447±0.015	0.439±0.015

Table 17: Bias Check For CMX Case

Input A_{fb}	A_{fb}^{meas} +CMX	A_{fb}^{meas} -CMX
-0.4	-0.486±0.024	-0.478±0.022
-0.2	-0.259±0.025	-0.256±0.023
-0.1	-0.14±0.03	-0.15±0.23
-0.05	-0.088±0.03	-0.1±0.02
0.0	-0.03±0.03	-0.04±0.02
0.05	0.032±0.03	0.013± 0.02
0.1	0.09±0.03	0.07±0.02
0.2	0.205±0.026	0.182±0.023
0.4	0.437±0.025	0.406±0.022

7 Systematic Uncertainties

A number of complicating effects contribute to our measurement uncertainty in a way that is not yet reflected in our calculation. These additional "systematic" uncertainties will account for the possible imprecision in several important inputs to our model. Each uncertainty is treated in its own way, but the common technique is to compare our baseline model with one where one of the inputs has been varied within its known error.

7.1 Jet Energy Scale

Several corrections are applied to the measured energy of jets inside the detector. These corrections account for the response of calorimeters to different particles, non-linear response of the calorimeters to particle energies, regions of the detector without instrumentation, and energy radiated outside the jet clustering algorithm. Error associated with the determination of these corrections is assigned as a systematic error to the analysis. Each individual uncertainty in the jet energy scale is listed below.

- Relative Correction
  Corrections due to η dependent calorimeter response.

- Underlying Event Correction
  Correcting for energy associated with the spectator partons in the event.

- Absolute Correction
  Corrects the jet energy measured in the calorimeter for any non-linearity and energy loss in the un-instrumented regions of each calorimeter.

- Out Of Cone Correction
  Corrects back to particle-level energy by accounting for leakage of radiation outside the jet clustering cone.

- Splash Out Correction
  Uncertainty in the energy leakage beyond the out of cone scope.

The uncertainty due to the jet energy scale could cause different portions of the detector to over or under correct the amount of energy in jets, and therefore create a bias in the measurement of the asymmetry. For example, if the forward region of the detector was overcorrected compared to the backward region this would cause an asymmetry in the measurement. If there is a bias in the jet energy scale as a function of η, the shape of the production angle distribution predicted by Monte Carlo could be distorted. The Monte Carlo may not correctly model the "real" complexities of the jet-parton assignment. The error in the jet energy scale would also be responsible for error in the correction matrices defined in Section 6.

The combined uncertainty of the jet energy scale is the quadrature sum of the individual uncertainties. A "shifted" sample is created by applying a scale factor to the energy of individual jets that represents a 1.0σ uncertainty in the jet energy scale. Two such samples are created: a $+1.0\sigma$ sample and a -1.0σ sample. The "jet energy shifted" samples and our default model are reweighted to have an asymmetry of 0.1. We then apply our measurement procedure to these samples and calculate the difference between the two shifted samples, and then calculate the difference between each shifted sample and the default sample. The largest value is taken as the systematic uncertainty.

Table 18: Jet Energy Scale Error

Event Type	$+\Delta$	$-\Delta$	Diff/2	$\lvert Max\rvert$
+CEM	-0.006	0.002	0.002	0.006
-CEM	-0.001	-0.005	-0.003	0.005
+CMUP	0.003	0.002	0.003	0.003
-CMUP	-0.003	0.006	0.002	0.006
+CMX	0.01	-0.015	-0.003	0.015
-CMX	-0.004	-0.001	-0.003	0.004
Combined				0.006

7.2 Background Shape

The shape of the production angle for each background component can be unique. Fluctuations in the relative contributions of each background will distort the overall shape of the background production angle, change the background asymmetry, and lead to an error in the background correction. We estimate the systematic uncertainty due to this effect by the technique of "pseudo-experiments".

Each "pseudo-experiment" contains approximately the number of signal and background events expected in our data sample. These events are drawn from our "models", as described in section 4, in an amount that represents Poisson fluctuations around the expected mean of each type. We pass these events through our full measurement procedure and record the resulting measured A_{fb}. If our procedure is correct, the resulting "spectrum" of A_{fb} from many pseudo-experiments should have a mean that represents the underlying true $t\bar{t}$ A_{fb} and a width that represents the statistical error on the measurement.

We perform this procedure with reweighted signal events ($A_{fb} = 0.1$) and events from the background models described in section 4. We produce three $+1.0\sigma$ shifted samples and three -1.0σ shifted samples by changing the normalization of the three largest backgrounds (QCD, $Wb\bar{b}$, W+LF) by a factor of 2 and 1/2. For each background, the largest difference between the default model and the shifted sample is taken as the systematic uncertainty. The combined systematic uncertainty for each lepton

category is the quadrature sum of the uncertainties for each background. The result of this procedure is shown in Table 19.

Table 19: Background Shape

Event Type	$+\Delta_{QCD}$	$-\Delta_{QCD}$	$+\Delta_{W+HF}$	$-\Delta_{W+HF}$	$+\Delta_{W+LF}$	$-\Delta_{W+LF}$	$\sum_{quad}$
+CEM	-0.016	0.004	0.002	0.0	-0.002	0.0	0.016
-CEM	0.009	0.003	-0.016	0.012	-0.014	0.01	0.023
+CMUP	-0.02	0.01	-0.003	-0.001	0.003	0.005	0.021
-CMUP	0.006	-0.012	-0.02	-0.002	-0.02	0.0	0.031
+CMX	-0.017	0.001	-0.002	0.01	-0.008	0.004	0.019
-CMX	-0.019	0.032	0.0	0.01	0.01	0.012	0.036
Combined							0.022

7.3 Initial State Radiation (ISR)

Initial state radiation in $t\bar{t}$ events consists of gluons that are radiated from the production particles before hard collision. If the radiated gluons are energetic enough they will produce a jet that can be misidentified as one of the partons from the $t\bar{t}$ decay. The physics of this process in $t\bar{t}$ events is not yet well measured or understood, which leads to an uncertainty in the amount of ISR affecting our measurement procedure.

To calculate the systematic error due to uncertainty in ISR, we generate two $t\bar{t}$ simulated samples where the amount of ISR is shifted by $+1.0\sigma$ and -1.0σ of the theoretical error. The shifted ISR samples are reweighted to have an asymmetry of 0.1 and compared to our default $t\bar{t}$ Monte Carlo sample, also reweighted with an asymmetry of 0.1. We calculate the difference between the two shifted samples, and calculate the difference between each shifted sample and the default sample. The largest value is taken as the systematic uncertainty.

7.4 Final State Radiation (FSR)

Final state radiation in $t\bar{t}$ events consists of gluons that are radiated from the final state particles. If the radiated gluons are energetic enough they will produce a separate jet. FSR produces measurement error because it creates two jets both from the same parton but with less energy. One of these jets can be used in reconstruction with mismeasured energy or both could enter reconstruction which would displace the "correct" jet from the reconstruction process. The physics of this process in $t\bar{t}$ events is not yet well measured, which leads to an uncertainty in the amount of FSR affecting our measurement procedure.

Table 20: ISR Error

Event Type	$+\Delta$	$-\Delta$	Diff/2	$\lvert Max\rvert$
+CEM	-0.01	0.026	0.08	0.026
-CEM	0.004	0.008	0.006	0.008
+CMUP	0.008	-0.003	0.006	0.008
-CMUP	-0.015	-0.006	0.005	0.006
+CMX	-0.014	-0.015	0.0	0.0015
-CMX	-0.065	-0.018	0.018	0.065
Combined				0.017

Table 21: FSR Error

Event Type	$+\Delta$	$-\Delta$	Diff/2	$\lvert Max\rvert$
+CEM	-0.001	-0.023	-0.012	0.023
-CEM	0.01	-0.01	0.001	0.01
+CMUP	0.042	0.028	0.04	0.042
-CMUP	-0.01	0.01	0	0.01
+CMX	-0.023	0.019	-0.002	0.023
-CMX	0.008	0.0	0.004	0.008
Combined				0.019

To calculate the systematic error due to uncertainty in FSR, we generate two $t\bar{t}$ simulated samples where the amount of FSR is shifted by $+1.0\sigma$ and -1.0σ of the theoretical error. The shifted FSR samples are reweighted to have an asymmetry of 0.1 and compared to our default $t\bar{t}$ Monte Carlo sample, also reweighted with an asymmetry of 0.1. We calculate the difference between the two shifted samples, and calculate the difference between each shifted sample and the default sample. The largest value is taken as the systematic uncertainty.

7.5 Mass Of The Top Quark

As described in section 5, the known mass of the top quark is used as a constraint in reconstruction. If the mass of the top quark is different from our constraint, the reconstruction is fitting the data to the wrong hypothesis.

Two Monte Carlo simulations of $t\bar{t}$ events, one with mass 175 GeV and the other with 178 GeV, are reweighted to produce $A_{fb} = 0.10$. The samples are passed through our measurement procedure, except background subtraction, and the difference is considered the systematic error. The result is shown in Table 22.

Table 22: Mass Error

Event Type	Difference
+CEM	0.009
-CEM	0.001
+CMUP	-0.004
-CMUP	0.026
+CMX	-0.001
-CMX	-0.026
Combined	0.009

Table 23: MC Gen Error

Event Type	Difference
+CEM	-0.015
-CEM	0.001
+CMUP	-0.008
-CMUP	0.041
+CMX	-0.005
-CMX	-0.07
Combined	0.016

7.6 Monte Carlo Generator

Monte Carlo is expected to model the $t\bar{t}$ process from production to final state particles. This requires a number of effects to be simulated properly, such as top quark production, top quark decay, and hadronization. Uncertainty in any number of these effects translates into uncertainty in our measurement. Fortunately, these simulations have been tested and refined over many measurements of many different processes. Nonetheless, we assign an uncertainty to our measurement to account for differences between our model and the actual $t\bar{t}$ process. We calculate the systematic error by comparing our measurement for two entirely different Monte Carlo simulations: Pythia and Herwig. Events from these two simulations are reweighted to produce an asymmetry of 0.1. The reweighted events are passed through our measurement procedure and the difference between the two measured values is taken as the systematic error. The result is shown in Table 23.

7.7 Parton Distribution Function (PDF)

The momentum distribution of partons and gluons in Monte Carlo simulations is derived from empirically calculated functions, called "PDF's". The momentum distribution of the particles in the hard scattering process determines the "energy" spectrum of the $t\bar{t}$ system. To study the effect on our measurement to the uncertainty in the PDF, we compare three different $t\bar{t}$ Monte Carlo samples generated with different PDF (CTEQ5L, MRST72, MRST75 [35] [36]) and reweighted to have an asymmetry equal to 0.1. The measurement procedure is applied to these three samples and the largest deviation of the measured value between any two samples is taken as the systematic uncertainty. The result is shown in Table 24.

7.8 Correcting A_{fb}

In testing our correction procedure in section 6.4.1, we observed a slight over-correction in the measurement of A_{fb} that increased as a function of the input A_{fb}. The effect is small, but is treated as a systematic error in the analysis. The difference between

Table 24: PDF Error

Event Type	CTEQ5L-MRST72	CTEQ5L-MRST75	MRST72-MRST74	$\|Max\|$
+CEM	-0.009	-0.009	0.0	0.009
-CEM	0.014	-0.007	0.011	0.014
+CMUP	0.021	0.008	-0.013	0.021
-CMUP	0.003	0.02	0.012	0.02
+CMX	-0.009	-0.009	0.0	0.009
-CMX	0.06	0.046	-0.014	0.06
Combined				0.015

the input A_{fb} and the corrected A_{fb} at an asymmetry equal to 0.2 is taken as the systematic uncertainty.

Table 25: Correcting A_{fb}

Event Type	Difference
+CEM	-0.017
-CEM	0.001
+CMUP	-0.03
-CMUP	0.01
+CMX	-0.005
-CMX	-0.06
Combined	0.02

7.9 Combined Systematic Uncertainty

The combined systematic uncertainty on the measurement of A_{fb} is calculated by adding each individual uncertainty in quadrature. The result is:

$$\sigma_{syst} = \pm 0.047 \tag{36}$$

8 Measurement

We now carry out the full method described in this note to measure the forward-backward asymmetry for 695 pb^{-1} of data collected at CDF. Candidate $t\bar{t}$ lepton plus jets events are selected in data from the high Pt lepton triggers, as described in **??**. The top production angle for each event is reconstructed using the algorithm described in 5, and the number of forward ($Cos(\Theta) > 0$) and backward ($Cos(\Theta) < 0$) events are counted. The predicted background contributions in the forward and backward hemispheres are subtracted. Bias and smearing are corrected with the procedure described in section 6. The front-back asymmetry is calculated from the corrected forward and backward counts by:

$$A_{fb} = \frac{N_{Forward} - N_{Backward}}{N_{Forward} + N_{Backward}} \tag{37}$$

This procedure is performed separately for events with $\pm CEM$ electrons, $\pm CMUP$ muons, and $\pm CMX$ muons. The asymmetries in each of these six categories are combined in a weighted average:

$$A_{fb} = \sum_{i=1}^{6} (-Q_l) \cdot A_{fb}^{i} \cdot \frac{N_{events}^{i}}{N_{events}^{Total}} \tag{38}$$

where i = $\pm CEM$, $\pm CMUP$, $\pm CMX$.

The step-by-step details of this procedure for 695 pb^{-1} of data collected at CDF are now described.

8.1 Event Selection

For the 695 pb^{-1} of data collected at CDF, 257 events are selected. The breakdown of those events into the type and charge of tight lepton found in the event is shown in Table 26. The data sample contains 154 events with a CEM electron, 72 with a CMUP muon, and 31 with a CMX muon. The number of positive to negative lepton events is almost equal, 126 to 131, as expected by charge conjugation symmetry, and the equality holds for all three lepton categories.

8.2 Reconstruction

The reconstruction algorithm is applied to events accepted from selection. A χ^2 cut at 50 is applied to remove poorly measured events. After the cut, 243 events remain from the original 257. The breakdown of these events among the six lepton categories is shown in Table 27.

The number of events in each category is reduced slightly or not at all by the χ^2 cut, and the relative contributions of each lepton category to the total number of events remain almost the same.

Table 26: Number Of Events By Lepton Category

Lepton Type	N_{Events}	% Of Total	N_{Events}^{Bkg}	Pred S/B
+CEM	77	30.0	12.43	6.2
-CEM	77	30.0	12.34	6.2
+CMUP	33	12.8	7.58	4.4
-CMUP	39	15.2	7.30	5.34
+CMX	16	6.2	3.50	4.6
-CMX	15	5.8	3.32	4.5

Table 27: Event Counts After χ^2 Cut

Lepton Type	N_{Events}	Cut Efficiency (%)	% Of Total
+CEM	72	93.5	29.6
-CEM	74	96.1	30.4
+CMUP	32	97.0	13.2
-CMUP	35	89.7	14.4
+CMX	16	100.0	6.6
-CMX	14	93.3	5.8

The reconstructed production angle distributions for all categories are shown in Figures 28 to 33 along with the predicted distribution for signal and backgrounds. The combined distribution, $(-Q_l) \cdot Cos(\Theta)$, is shown in Figure 34. The shape of the production angle for each individual category and the combined data are in reasonable agreement withthe model prediction. The front-back asymmetry in each of these distributions is shown in Table 28.

Table 28: A_{fb} After Reconstruction

Lepton Type	N_{Events}^{Recon} F-B	A_{fb}^{Recon}
+CEM	39-22	0.08±0.12
-CEM	42-32	0.14±0.12
+CMUP	10-22	-0.38±0.16
-CMUP	20-15	0.14±0.17
+CMX	9-7	0.13±0.25
-CMX	9-5	0.29±0.26

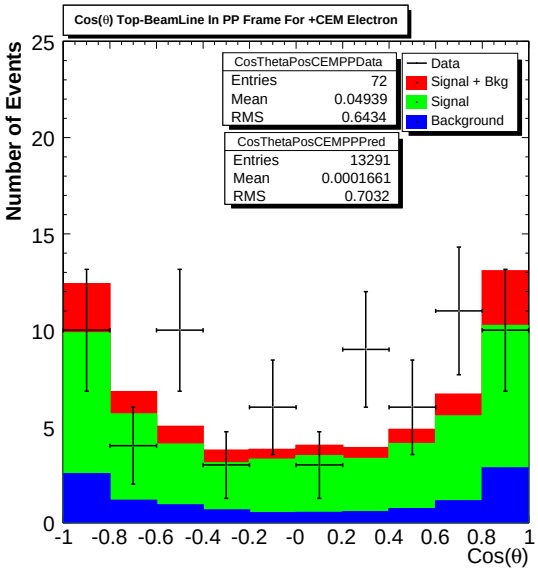

Figure 28: + Electron (CEM) $Cos(\Theta)$ Distribution

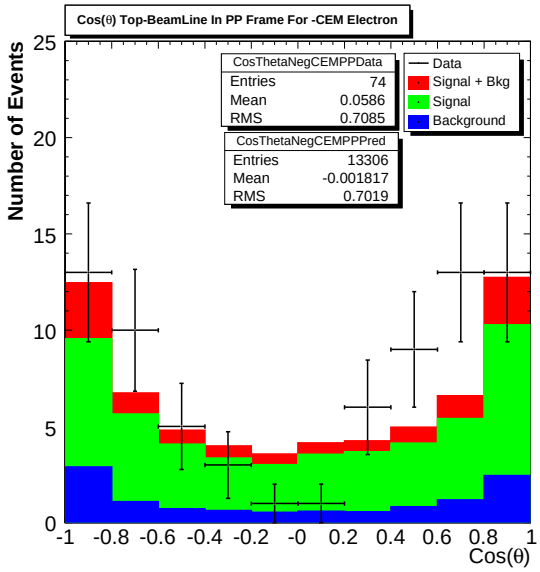

Figure 29: - Electron (CEM) $Cos(\Theta)$ Distribution

As we showed previously in section 5.3.6, the combined asymmetry is:

$$A_{fb}^{recon} = 0.095 \pm 0.063 \tag{39}$$

Recall from section 5 that the raw predicted value from the model is 0.010±0.006.

Looking at the separate lepton categories, we see that the non-zero value of the asymmetry is mostly due to a large asymmetry in events with a CMUP muon. For events with a CMUP muon:

$$A_{fb}^{+CMUP} = -0.38 \pm 0.16$$
$$A_{fb}^{-CMUP} = 0.14 \pm 0.17$$
$$A_{fb}^{CMUP} = -A_{fb}^{+CMUP} + A_{fb}^{-CMUP} = 0.25 \pm 0.12$$

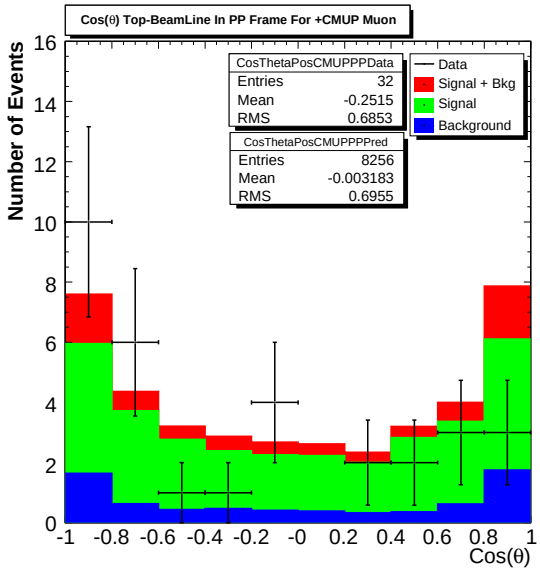

Figure 30: + Muon (CMUP) $Cos(\Theta)$ Distribution

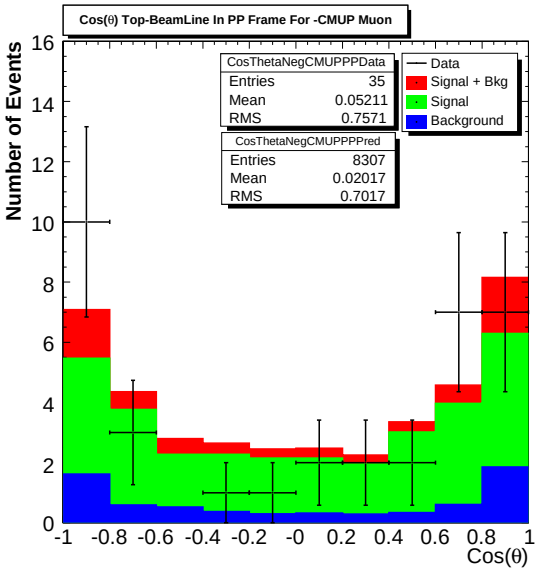

Figure 31: - Muon (CMUP) $Cos(\Theta)$ Distribution

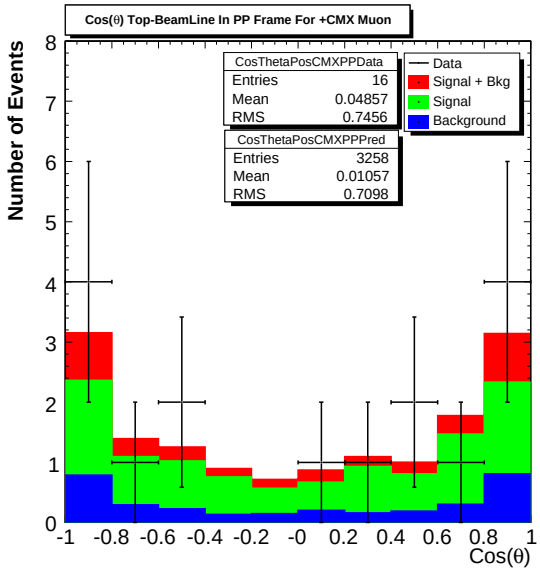

Figure 32: + Muon (CMX) $Cos(\Theta)$ Distribution

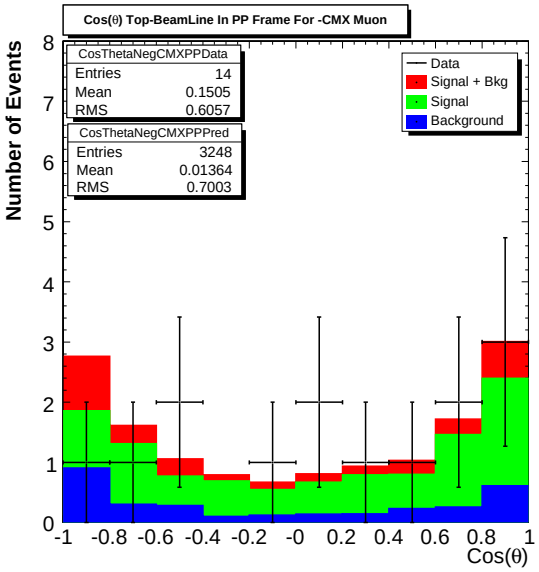

Figure 33: - Muon (CMX) $Cos(\Theta)$ Distribution

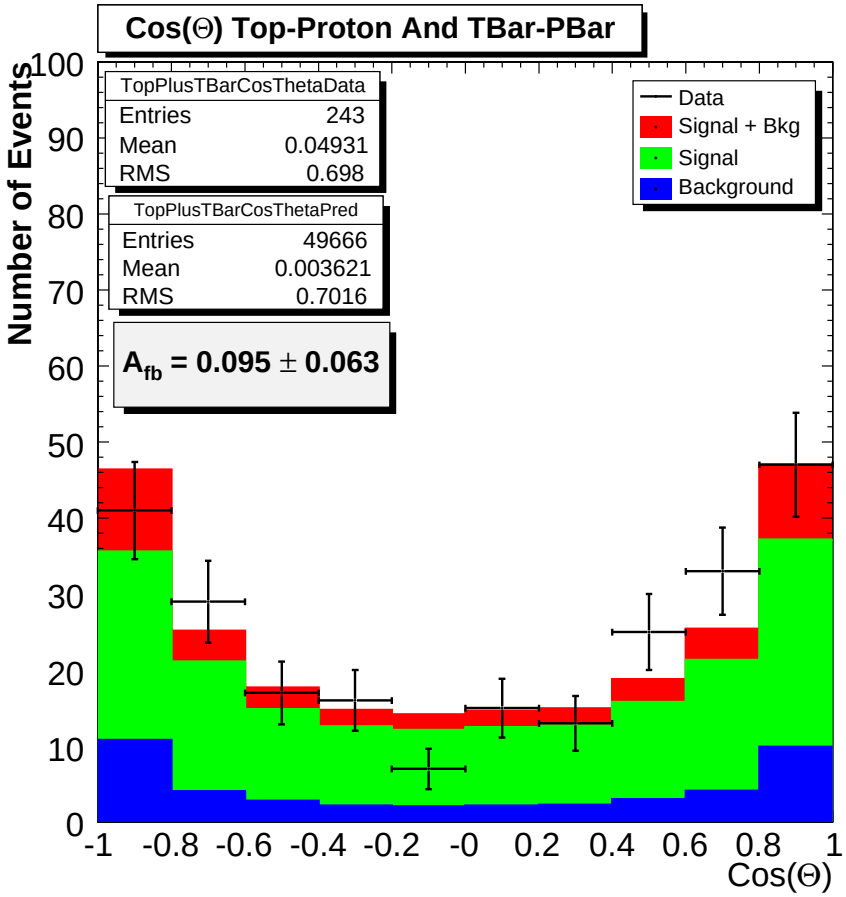

Figure 34: Combined Distribution

8.3 Correcting For Backgrounds

The predicted amount of background content in the forward/backward regions is subtracted from data for each of the six lepton categories. Table 29 shows the number of forward-backward events before and after subtraction and the background corrected asymmetry for each category. Because of the relatively small asymmetry in backgrounds, background processes for $t\bar{t}$ lepton plus jets events dilute, as opposed to bias, the measurement. The result is an increase in A_{fb} after correction in each category. The combined asymmetry after background subtraction is:

$$A_{fb}^{recon} = 0.126 \pm 0.078 \tag{40}$$

Table 29: Forward-Backward Asymmetry After Background Subtraction

Lepton Type	N_{Events}^{Recon} F-B	N_{Events}^{Bkg} F-B	$N_{Events}^{bkg-sub}$	$A_{fb}^{bkg-sub}$
+CEM	39-22	6.21-6.22	32.8-26.8	0.10±0.14
-CEM	42-32	6.04-6.30	36.0-25.7	0.17±0.14
+CMUP	10-22	3.72-3.86	6.28-18.1	-0.49±0.22
-CMUP	20-15	3.66-3.64	16.3-11.4	0.18±0.21
+CMX	9-7	1.79-1.71	7.2-5.3	0.15±0.32
-CMX	9-5	1.48-1.84	7.5-3.2	0.41±0.34

8.4 Correcting For Acceptance And Reconstruction

The correction procedure, equation 41 in section 6, is applied to the background corrected forward-backward values in Table 29 as shown below.

$$\begin{bmatrix} F_{corr} \\ B_{corr} \end{bmatrix} = M_{corr} \cdot \begin{bmatrix} F_{bkgsub} \\ B_{bkgsub} \end{bmatrix} \tag{41}$$

F_{bkgsub} and B_{bkgsub} are the number of background corrected forward and backward events, M_{corr}^{i} are the correction matrices for each lepton category i, and F_{corr} and B_{corr} are the final corrected forward and backward events. The resulting corrected forward backward asymmetries are shown in Table 30.

Because the detector and event selection are close to symmetric, the largest correction is for smearing effects in reconstruction. Smearing dilutes any underlying asymmetry that is present in the data and, therefore, applying the corrections increases the reconstructed asymmetry as is seen in Table 30 when compared to Table 29.

The final combined result, which is comparable to the predicted Standard Model value, 0.038, is:

$$A_{fb} = 0.20 \pm (0.11)^{stat} \pm (0.047)^{syst}$$

Lepton Type	A_{fb}^{corr}
+CEM	0.13±0.19
-CEM	0.27±0.19
+CMUP	-0.69±0.30
-CMUP	0.28±0.29
+CMX	0.17±0.46
-CMX	0.58±0.46

Table 30: Forward-Backward Asymmetry After Background Subtraction

9 Conclusion

We have developed a method of reconstructing $t\bar{t}$ events in the lepton plus jets mode and applied this to a measurement of the front-back asymmetry in top production in 695 pb^{-1} of proton-antiproton collisions at $\sqrt{s} = 1.96$ TeV. The measurement is a test of charge symmetry in the strong interaction at large momentum transfer. In the present data set it is also potentially sensitive to large parity violating contributions to top production. The measured front-back asymmetry, which is an be compared to the predicted Standard Model value, 0.038, is:

$$A_{fb} = 0.20 \pm (0.11)^{stat} \pm (0.047)$$

The measured asymmetry is marginally consistent with the theoretical prediction, and the shape of the combined production angle distribution in data is consistent with our model. The largest contribution to the asymmetry arises in events with a CMUP muon. In CMUP we find 0.48 ± 0.21. In electrons we find 0.071 ± 0.13. In CMX muons we find 0.18 ± 0.32. For events where the negatively charged top quark production angle is used, we find 0.084 ± 0.15. For events where the positively charged production angle is used, we find 0.31 ± 0.15. We have re-examined the CMUP sample and see nothing alarming in any other validation quantities. Our study of the front-back symmetry of the detector does not lead us to expect a systematic effect of this size in the muon system. Whether the effect is an unanticipated peculiarity of the CDF muon system or a statistical fluctuation or a real asymmetry can only be ascertained by study with a larger data set. All lepton categories have a positive asymmetry except events with

a negative CMUP muon. The asymmetry should have equal and opposite magnitudes for t and $\bar{t}$, assuming CP symmetry. Our statistical precision insufficient to see this expected result.

Larger data sets at the LHC will be sensitive to an interesting charge asymmetry arising from pure QCD at NLO, expected to be of order 3.8%. The measurement procedure at the LHC will be complicated by the fact that the colliding particles there are proton-proton and therefore, the dominant production mechanism of $t\bar{t}$ pairs is gluon fusion, which has no asymmetry. Kuhn and Rodrigo have suggested an alternative measurement which will be sensitive to the QCD asymmetry, assuming several new obstacles can be overcome in the analysis [33].

We intend to update this measurement with 1 fb^{-1} of data within the coming months and to publish the result.

References

[1] F.Abe et al., "Observation of the Top Quark in $p\bar{p}$ Collisions with the CDF Detector at Fermilab", Phys. Rev. Letters 74, 2626 (1995).

[2] M.Cacciari et al., JHEP 0404, 68 (2004)

[3] M.Beneke et al., "Top Quark Physics", CERN-TH-2000-100 (2000)

[4] A. Abulencia et al., CDF Collab., CDF conference note 7712 (2005).

[5] W. Pauli, "Niels Bohr and the Development of Physics", McGraw-Hill, NY (1955)

[6] J. H. Christenson, J. W. Cronin, V. L. Fitch, and R. Turlay, "Evidence for the 2π Decay of the K_2^0 Meson",Phys. Rev. Letters 13, 138 (1964).

[7] C.S Wu et al., "Experimental Test of Parity Conservation in Beta Decay", APS Phys Rev 105, 141301415 (1957).

[8] A. Angelopoulos et al. (CPLEAR collaboration),"First direct observation of time-reversal non-invariance in the neutral kaon system", Phys.Lett. B 444 (1998) 52.

[9] M.Carena, A.Daleo, B.A.Dobrescu, T.Tait, "Z' Gauge Bosons At The Tevatron", hep-ph/0408098 (2004).

[10] C.T. Hill, "Topcolor Assisted Technicolor", Phys. Lett. B 345, 483 (1995).

[11] S.Edielman et al., "Review of Particle Physics", Phys. Lett. B 592, 1 (2004).

[12] R. Erbacher et al., "Preliminary Event Selection and $t\bar{t}$ Signal Acceptance of the Winter 2005 Top Lepton + Jets Sample", CDF Note 7372

[13] D. Acosta et al., "Measurement of the t anti-t production cross section in p anti-p collisions at $\sqrt{s} = 1.96$ TeV using lepton plus jets events with secondary vertex b-tagging", hep-ex/0411041.

[14] T. Affolder et al., Phys Rev D 64, 032002 (2001).

[15] A. Abulencia et al., CDF Collab., CDF conference note 8110 (2006), submitted to Phys. Rev. Lett.

[16] A. Holloway et al., "SecVtx Scale Factor Measurement For Gen5 Tagger", CDF Note 7333

[17] A. Foland et al., "Preliminary Method 2 Backgrounds For Top Pair Production In Lepton Plus Jets Events With SecVtx Using 318.5 pb^{-1} Of $p\bar{p}$ Data", CDF Note 7486

[18] Joao Guimaraes da Costa and S. Rappoccio,"SecVtx Tag Matrices for 5.3.3nt", CDF Note 7326

[19] T. Sjostrand, S. Mrenna, and P. Skands. "Pythia 6.4: Physics and Manual", hep-ph/0603175 (2006).

[20] G. Corcella, I.G. Knowles, G. Marchesini, S. Moretti, K. Odagiri, P. Richardson, M.H. Seymour and B.R. Webber, "Herwig 6.5", JHEP 0101 (2001) 010, hep-ph/0011363 and hep-ph/0210213.

[21] S. Frixione and B.R. Webber, "Matching NLO QCD computations and parton shower simulations", JHEP 0206 (2002) 029 [hep-ph/0204244]
S. Frixione, P. Nason and B.R. Webber, "Matching NLO QCD and parton showers in heavy flavour production", JHEP 0308 (2003) 007 [hep-ph/0305252]

[22] F. Maltoni and T. Stelzer, JHEP 0302:027,2003
T. Stelzer and W.F. Long, Phys. Commun. 81 (1994) 357-371
H. Murayama, I. Watanabe, and K. Hagiwara, 1991

[23] M.L. Mangano, M. Moretti, F. Piccinini, R. Pittau, A. Polosa, "ALPGEN, a generator for hard multiparton processes in hadronic collisions", JHEP 0307:001,2003, hep-ph/0206293.

[24] D. Acosta et al., The CDF Collaboration, Phys. Rev. D71, 051104 (2005).

[25] F.James, "MINUIT: Function Minimization and Error Analysis Reference Manual", http://wwwasdoc.web.cern.ch/wwwasdoc/minuit/minmain.html, Computing And Networks Division, CERN (1998).

[26] CDF and D0 Collaborations, and the Tevatron Electroweak Working Group ,hep-ex/0603039 (2006).

[27] A. Abulencia et al., CDF Collab., CDF conference note 7794 (2005), submitted to Phys. Rev. Lett.

[28] D0 Collab., D0 conference note 4833 (2005).

[29] A. Abulencia et al., CDF Collab., CDF conference note 7804 (2005), Submitted to Phys. Rev. Lett.

[30] CDF Collaboration., CDF conference note 8087(2006).

[31] D. McGinnis et. al, "The Run II Handbook", Tech.Rep. http://www-ad.fnal.gov/runII", Fermilab Accelerator Devision, 2000.

[32] D. Amidei, "The CDF II Detector, Technical Design Report", Tech.Rep. FERMILAB-PUB-96-390-E, Fermi National Accelerator Laboratory, 1996.

[33] J.H. Kuhn and G. Rodrigo, Phys. Rev. Lett. 81, 49 (1998)
J.H. Kuhn and G. Rodrigo, Phys. Rev. D 59, 054017(1999).

[34] CDF Collaboration, CDF Conference Note 8125 (2006). http://www-cdf.fnal.gov/

[35] J.Pumplin et al., JHEP, 012 (2002)

[36] R.D.Field, See talks available at http://www.phys.ufl.edu/rfield/cdf/.